DOKUZ EYLÜL UNIVERSITY
GRADUATE SCHOOL OF NATURAL AND APPLIED SCIENCES

INVESTIGATION OF CORROSION PROPERTIES OF NI MATRIX NANOCOMPOSITE COATINGS PRODUCED BY ELECTRODEPOSITION TECHNIQUE

by
Tülay KOÇ DELİCE

January, 2018
İZMİR

INVESTIGATION OF CORROSION PROPERTIES OF NI MATRIX NANOCOMPOSITE COATINGS PRODUCED BY ELECTRODEPOSITION TECHNIQUE

A Thesis Submitted to the
Graduate School of Natural and Applied Sciences of Dokuz Eylül University
In Partial Fulfillment of the Requirements for the Degree of Master of Science in Department of Nanoscience and Nanoengineering

by
Tülay KOÇ DELİCE

January, 2018
İZMİR

M.Sc THESIS EXAMINATION RESULT FORM

We have read the thesis entitled **"INVESTIGATION OF CORROSION PROPERTIES OF NI MATRIX NANOCOMPOSITE COATINGS PRODUCED BY ELECTRODEPOSITION TECHNIQUE"** completed by **TÜLAY KOÇ DELİCE** under supervision of **ASST. PROF. DR. N. FUNDA AK AZEM** and we certify that in our opinion it is fully adequate, in scope and in quality, as a thesis for the degree of Master of Science.

.....

Asst. Prof. Dr. N. Funda AK AZEM

Supervisor

.....

Yrd. Doç. Dr. Işıl BİRLİK

(Jury Member)

.....

Doç. Dr. Osman CİLİNGİR

(Jury Member)

Prof. Dr. Kadriye ERTEKİN

Director

Graduate School of Natural and Applied Sciences

ACKNOWLEDGMENTS

I would like to express my heartfelt gratitude to my advisor Assist. Prof. Dr. N. Funda AK AZEM and co-advisor Assist. Prof. Dr. Işıl BİRLİK for their guidance, enthusiasm, patience, motivation, and enormous knowledge throughout my master's study.

I would also like to acknowledge Ramazan DALMIŞ, Şükrü KAYA, Dalyan ÖZKAN, Serhan KÖKTAŞ, Haydar KAHRAMAN, Kadir Cihan TEKİN, Tuncay DİKİCİ, Ahmet Çağrı KILINÇ and Metin YURDDAŞKAL for the stimulating discussions, for their help during my master's studies and making research lab being a nice place to work. I would like to extra thank my friends Bensu BAKIN and Oylum ÇOLPANKAN GÜNEŞ for helping me in dealing with stress and giving emotional support throughout my studies. In addition, I would like to thank Utku TİRİÇ, Sıdıka YILDIRIM and Onur BARDAKÇIOGLU for their invaluable assistance and kind friendship. The present research was also supported by The Scientific and Technological Research Council of Turkey (TÜBİTAK) with project code 113R023 named as "Production, investigation and industrial utilization of nanocomposite coatings as photoanode applications for cathodic protection systems" and scientific research project (BAP) with project code 2014.KB.FEN.046 named as "Investigation of corrosion properties of Ni matrix nanocomposite coatings produced by electrodeposition technique".

Finally, a special thank goes to my family for their concern, confidence and support. I extend my greatest thanks to my husband Kılıç DELİCE who has been immeasurably receptive, incentive and patient with me during this time. And I present my eternal love for being with me every moment to my most precious, my unique son, Baki Musab Ömer DELİCE presents my eternal love for being with me every moment. No word can do justice to my appreciation for them.

Tülay KOÇ DELİCE

INVESTIGATION OF CORROSION PROPERTIES OF NI MATRIX NANOCOMPOSITE COATINGS PRODUCED BY ELECTRODEPOSITION TECHNIQUE

ABSTRACT

This research aimed to investigate electrochemical corrosion behavior of Nickel matrix nanocomposite coatings produced by electrodeposition technique in a Watts bath containing titanium dioxide and Zinc doped titanium dioxide nanoparticles.

In this study, titanium dioxide and Zinc doped titanium dioxide nanoparticles were prepared using a sol-gel method. Obtained results indicate that all synthesized nanoparticles and particle sizes were below 100 nm. Nickel matrix nanocomposite coatings were produced by using electrochemical deposition tecnique on stainless steel substrates. The Watts bath for production of nanocomposite coatings were prepared using the different amounts of titanium dioxide and Zinc doped titanium dioxide nanoparticles. Besides, applied current density on the coating performance were investigated in order to optimize the coating properties. Pure Nickel coatings were also deposited under the same experimental conditions for comparison.

The structural, morphological, mechanical and corrosion properties of the Nickel matrix nanocomposite coatings were investigated. The surface morphology, elemental composition and phase structure of the nanocomposite coatings were examined by Scanning Electron Microscopy, Energy Dispersive Spectrometer and X-ray Diffraction, respectively. Obtained results show that Nickel-Titanium dioxide and Nickel- Zinc/Titanium dioxide nanocomposite coatings improved corrosion properties.

Keywords: Nanoparticle, sol-gel, nickel coating, nanocomposite, electrodeposition, corrosion

ELEKTROÇÖKTÜRME TEKNİĞİ İLE ÜRETİLEN Nİ MATRİS NANOKOMPOZİT KAPLAMALARININ KOROZYON ÖZELLİKLERİNİN İNCELENMESİ

ÖZ

Bu araştırma, Titanyumdioksit ve Zinc katkılı titanyum dioksit nanopartikülleri içeren bir Watts banyosunda elektroçöktürme tekniği ile üretilen Nikel matriks nanokompozit kaplamaların elektrokimyasal korozyon davranışını araştırmayı amaçlamıştır.

Bu çalışmada, sol-jel yöntemi kullanılarak Titanyumdioksit ve Zinc katkılı Titanyumdioksit nanopartiküller hazırlandı. Elde edilen sonuçlar, sentezlenen tüm nanopartiküllerin homojen olarak sentezlendiğini ve partikül boyutlarının 100 nm'nin altında olduğunu göstermektedir. Nikel matris nanokompozit kaplamalar, paslanmaz çelik yüzeylerde elektrokimyasal çöktürme tekniği kullanılarak üretilmiştir. Nanokompozit kaplamaların üretimi için Watts banyosu, farklı miktarda titanyum dioksit ve Zinc katkılı titanyumdioksit nanopartiküller kullanılarak hazırlanmıştır. Ayrıca kaplama özelliklerini optimize etmek için kaplama performansı üzerine uygulanan akım yoğunluğu araştırılmıştır. Karşılaştırma için de saf Nikel kaplamalar aynı deney koşulları altında yapılmıştır.

Nikel matriks nanokompozit kaplamaların yapısal, morfolojik, mekanik ve korozyon özellikleri araştırılmıştır. Nanokompozit kaplamaların yüzey morfolojisi, elementel kompozisyonu ve faz yapısı, sırasıyla, Taramalı Elektron Mikroskopisi, Enerji Dağılımlı Spektrometre ve X-ışını Kırınımı ile incelenmiştir. Elde edilen sonuçlar, Nikel-Titanyumdioksit ve Nikel-Çinko/Titanyumdioksit nanokompozit kaplamaların korozyon özelliklerini iyileştirdiğini göstermektedir.

Anahtar Kelimeler: Nanopartikül, sol-jel, nikel kaplama, nanokompozit, elektroçöktürme, korozyon

CONTENTS

Page

LIST OF FIGURES

Page

LIST OF TABLES

Page

CHAPTER ONE
INTRODUCTION

Nanotechnology has created a key revolution in the twenty-first century, exploiting the new properties, phenomena, and functionalities exhibited by matters when dealt at the level of few nanometers. The nanometer scale is conventionally defined as 1 to 100 nm. At this level, the physical, chemical, and biological properties of materials differ in fundamental and valuable ways from properties of individual atoms and molecules or bulk matter. Nanophase and nanostructured materials constitute a new branch of material research and attract a great deal of attention because of their potential applications in areas such as coatings, electronics, optics, catalysis, ceramics, magnetic data storage, and polymer nanocomposites (S. A. Kumar & Denchev, 2009)

A major group of bulk nanostructured coatings is nanocomposites composed of a matrix filled with nanostructures of any category. Nanoparticles, nanotubes, nanowires, nanorods, nanosheets, etc. of any desirable material are distributed into a metal or non-metal matrix. This combines the capabilities of either constituent to achieve novel and unique properties and applications. Nanocomposites are classified into three main groups as metal matrix nanocomposites; ceramic matrix nanocomposites and polymer matrix composites (Nasirpouri, 2017).

Particle-reinforced metal matrix composite (MMC) coatings have been used in many engineering applications due to excellent mechanical properties. In composite materials, the metal matrix properties are modified by addition of various insoluble substances e.g. hard oxides as Al_2O_3, ZrO_2, SiO_2, TiO_2, carbides SiC and WC, diamond or solid lubricants (graphite, MoS_2 or PTFE). Many metals, such as nickel, copper, chromium, zinc, cobalt or alloys were mainly used as a metallic matrix. Among others nickel has been widely used, due to its resistant to corrosion and abrasion (Bełtowska-Lehman, Goral, & Indyka, 2011). Nickel matrix composite coatings containing nano-particles that exhibit excellent properties, such as higher wear and corrosion resistance, higher hardness, and more excellent self lubricating compared to metal coating (Rusu, Cojocaru, Magagnin, Gheorghies, & Carac, 2010). Nanocomposite nickel coatings

containing hard nanosized particles such as TiO_2, SiC, Al_2O_3, Si_3N_4, ZrO_2 and diamond can be readily electrodeposited. Reza Arghavanian et al. studied the effect of co-electrodeposited ZrO_2 particles on the microstructure and corrosion resistance of Ni coating and reported that higher ZrO_2 content in the coating results better corrosion resistance.

There are a number of methods of producing metal matrix composites such as electroless deposition, electroless plating, chemical and physical vapor depositon (Ghaziof & Gao, 2015). Amongst all these methods, electrodeposition, as a low-temperature, cheap and simple method, is a superior technique for preparation of nanocrystalline metals and alloys as well as nanocomposite coatings in a single step without secondary treatment. Electrochemical deposition shows also the additional advantages such as high deposition rate, simple equipment, the automation possibility, easy control of microstructure and thickness (from nanometers up to several tens of micrometers) of deposits plated uniformly on substrates of complicated shapes and large surfaces (Bełtowska-Lehman et al., 2011).

This study relates to the development of Ni-TiO_2 and Ni-Zn/TiO_2 nanocomposite caotings on steel substares for improved corrosion applications.

CHAPTER TWO
NICKEL AND NICKEL MATRIX NANOCOMPOSITE COATINGS

2.1 Introduction

The Nickel deposits are used in the industry to improve wear and corrosion resistance, to repair eroded metals, to improve magnetic properties, to prepare the substrate surface for glazing or producing the organic coating, and other purposes (Davis, 2000). Nickel has been widely used as metal matrix (Ren & Haeri, 2016). Nano composite electrodeposition is a method of codeposition nanometer size particles into different matrixes to improve material properties. Over the past decades, many studies has been focused on successful co-deposition of different types of particles such as oxide, carbide, polymer, nitride, diamond, graphite and metallic particles (Pereira, Oliveira, Vieira, Lima, & Urtiga Filho, 2017).

2.1.1 Hardness

Hardness of material is defined as the resistance of a material to deformation particularly permanent deformation, indentation or scratching (Bailey et al., 2003; Dieter & Bacon, 1986).

Ceramic particle addition to nickel coatings acts as a barrier to dislocation movement and increases a hardness of the composite coatings. Effect of reinforced particles in composite coatings on hardness depends mainly on volume content as well as size and distribution of these particles in the metal matrix (W. Wang, Hou, Wang, & Guo, 2005). The smaller particles produced a larger hardening effect and the strengthening mechanism was explained by a combination of the Orowan-type strengthening and Hall-Petch effects. Increament in the hardness of nickel nanocomposite film is associated with the presence of the intrinsic hardness of the codeposited ceramic phase, to a dispersion hardening and to the refinement of the microstructure (V. Singh & Singh, 2014).

2.1.2 Corrosion Resistance

Nickel composite coatings have better corrosion resistance than pure nickel coatings because reinforced second phase particles disturb the regular growth of nickel crystal and promote new nucleation site (Amadeh, Rahimi, Farshchian, & Moradi, 2010; Szczygieł & Kołodziej, 2005). Addition of these particles in composite coatings will decrease corrosion current density and will shift corrosion potential of composite coatings towards more noble direction i.e. positive value.

2.1.3 Wear Resistance

Nickel composite coatings reinforced with Al_2O_3 (L. Chen, Wang, Zeng, & Xu, 2006), WC (Surender, Basu, & Balasubramaniam, 2004), TiO_2 (Baghery, Farzam, Mousavi, & Hosseini, 2010), ZrO_2 (W. Wang et al., 2005), CNTs (Arai, Fujimori, Murai, & Endo, 2008), SiC(Hou, Ger, Wang, & Ke, 2002), and Si_3N_4 (Srivastava, Grips, & Rajam, 2008) show better wear resistance compared to pure nickel coatings.

These reinforced second phase particles in the nickel matrix act as a physical barrier to nickel grain growth and plastic deformation of nickel matrix under loading promotes grain refining and dispersive strengthening and therefore, they improve the wear resistance of composite coatings (Vaezi, Sadrnezhaad, & Nikzad, 2008).

2.1.4 Applications of Nickel Composite Coatings

Nickel composite coatings are widely used in applications which require abrasion and heat resistant coatings, corrosion resistant coatings, self lubrication films and thermally graded structures (Shao, Vereecken, Chien, Searson, & Cammarata, 2002). For example, small aircrafts, microdevices and coatings of engine cylinders and high pressure valves are some of the application areas of Ni-Al_2O_3 composite coatings (Szczygieł & Kołodziej, 2005). In combustion engine and casting moulds, Ni-SiC composite coatings are mostly used and preferred (Vaezi et al., 2008). Due to excellent anti-wear property of Ni-CNT composite coatings, they can be find an application area

in the aerospace, automobile, and other industries as frictional components (An, Li, & Li, 2008).

CHAPTER TRHEE
SYNTHESIS OF NANOPARTICLES

3.1 General Introduction to Nanoparticles

In general, the size of a nanoparticle spans the range between 1 and 100 nm. Metallic nanoparticles have different physical and chemical properties from bulk metals (e.g., lower melting points, higher specific surface areas, specific optical properties, mechanical strengths, and specific magnetizations), properties that might prove attractive in various industrial applications. However, how a nanoparticle is viewed and is defined depends very much on the specific application. The most common nanoparticles currently implemented have been made of transition metals, silicon, carbon, and metal oxides. Among nanoparticles, metal oxide nanoparticles are attracting considerable interest due to their unique physical and chemical properties (Niederberger & Pinna, 2009). These metal oxide nanoparticles can be composed of a variety of materials for example: zinc oxide (ZnO), titaniumdioxide (TiO_2), copper oxide (CuO), zirconium dioxide (ZrO_2), Aluminum oxide (Al_2O_3), silicon dioxide (SiO_2), iron oxide (Fe_3O_4), magnesium oxide (MgO), nickel oxide (NiO), manganese dioxide(MnO_2) and etc.

Metal oxide nanostructures, such as TiO_2, ZnO, WO_3, and SnO_2, CuO nanostructures have other unique magnetic and super-hydrophobic (Liu, Jiang, Li, Zhang, & Ren, 2010) properties. Furthermore, these nanostructures show very promising applications in heterogeneous catalysis in the complete conversion of hydrocarbons into carbon dioxide, enhancement of thermal conductivity of nanofluid, nanoenergetic materials, and super-hydrophobic surfaces or anode materials for lithium ion batteries.

CuO, categorized into transition metal oxide group, is a p type, narrow band gap semiconductor ~1.7 eV (Nagajyothi, Muthuraman, Sreekanth, Kim, & Shim, 2017). It has monoclinic structure and many interesting characteristics: super thermal conductivity, photovoltaic properties, high stability, and antimicrobial activity. Due to

such exclusive properties, CuO can be used in many technological fields, for example, active catalyst (Yecheskel, Dror, & Berkowitz, 2013), gas sensor (Aslani & Oroojpour, 2011), high efficiency thermal conducting material (X. Wang, Xu, & S. Choi, 1999), magnetic recording media (Ishio et al., 2012) with very good selectivity, or solar cell applications (V. Kumar et al., 2013).

Nanostructured zirconia (ZrO_2) as one of the most industrially important materials has aroused interest owing to its thermal stability, chemical inertness, and lack of toxicity; thus, found to have a broad range of applications (Teymourian, Salimi, Firoozi, Korani, & Soltanian, 2014) . It is a widely utilized material which finds application in numerous fields such as high-performance ceramics, catalysts, sensors and optical devices. It has been employed in a wide variety of applications due to its excellent physical properties, which include, low thermal conductivity, high coefficient of thermal expansion, optical transparency, high strength, high fracture toughness, polymorphic nature and high thermal shock resistance amongst others.It provides an ideal host material for photonic applications, since its low phonon energy (470 cm^{-1}) decreases the probability of non-radiative multi-phonon relaxation of excited rare earth activator ions throughout the vibrational bands of the host lattice (Y. Chen, Lunsford, & Dionysiou, 2009; Tiwari, Kuraria, & Kuraria, 2015).

Al_2O_3 nanoparticle is also a new class of advanced and stable inorganic materials with very interesting features and capacity such as hydrophilic characteristic, non-toxic, highly abrasive and resistant and inexpensive which has been utilized in ultra-filtration membrane for water treatment (Hosseini et al., 2014). Remarkably, the use of alumina nanoparticles in membranes, especially in polymaide membrane synthesis by interfacial polymerization, has not yet been investigated to a large extent, in spite of their wide availability and applications in water treatment technology (Saleh & Gupta, 2012).

Silica nanoparticles have received an intensive attention of scientific community due to its wide applications in as electronic devices, insulator, catalysis or pharmaceuticals. Amorphous SiO_2 nano-particles are used in production of electronic

substrates, thin film substrates, electrical insulators, thermal insulators and humidity sensors (Giesche, 1994). It is essential to have silica particles of a narrow size distribution and a high purity, as high-tech industries such as biotechnology and photonics provide a tremendous demand for such materials (Vacassy, Flatt, Hofmann, Choi, & Singh, 2000). The optical properties of silica nanoparticles can be attained with respect to surface defect related to large surface/volume ratio (Dubey, Rajesh, & More, 2015).

Zinc Oxide (ZnO), a semiconductor with a band gap of 3.37 eV at room temperature, has had its catalytic properties studied extensively as it has a low cost, high photochemical reactivity, and because it is not toxic to environment. ZnO nanostructures have a great advantage when applied in photocatalytic reaction processes given their large surface area, high catalytic activity (Nava et al., 2017).The ZnO is an important semiconductor material due to its various applications. The nanoscale ZnO posses good photoelectric, optical and piezoelectric properties those can be useful for solar cell, gas sensor, acoustic wave resonator, optoelectronic application, photocatalyst etc (Suryawanshi, Bachhav, & Patil, 2015; Yamamoto, Otani, Seto, Nartpochananon, & Charinpanitkul, 2012).

Titanium nanoparticles are one of the most important metal oxide nanoparticles compared to others and are used in glass ceramics, electrical ceramics, catalyst, solar cell sensors, electric conductors and chemical intermediates (Sivaranjani & Philominathan, 2016). Among the semiconductor photocatalysts, titanium dioxide nanoparticles (TiO_2 NPs) has attracted numerous interests because of its excellent physicochemical properties, such as suitable band position, non-toxicity, low cost, chemical and photonic stability, and biocompatibility (Atchudan, Edison, Perumal, Karthikeyan, & Lee, 2017; Qiao et al., 2016).

Additionally, it is chemically inert, stable toward corrosion and photocorrosion, as well as inexpensive. TiO_2 nanoparticle are also used as food color additives and flavor enhancers (Weir, Westerhoff, Fabricius, Hristovski, & Von Goetz, 2012) and in various cosmetics owing to their ability to absorb and scatter UV light (Subramanian,

Wolf, & Kamat, 2003; Yang et al., 2013)). Due to their photocatalytical properties titania can additionally be employed in the degradation of pollutants in water treatment implants (Nurlaela, Chong, Dutta, & Riaz, 2010)

Unfortunately, the use of the bare TiO_2 phases presents some drawbacks that limit its application as a general tool, such as low quantum efficiency in the visible region (Adesina, 2004), high recombination rate for the photo produced electron–hole pairs and low transfer rate between photoelectron and oxygen molecule. The threshold wavelength corresponding to the band-gap energy of 3.2eV is at near ultraviolet radiation (387nm) for bare TiO_2, as a consequence, only 4% energy of the solar spectrum can be utilized (Leary & Westwood, 2011). Therefore, it's imperative to develop efficient photo catalysts which are more competitive against these drawbacks in this field and enhance photocatalytic efficiency, particularly under visible-light irradiation. In last years, various attempts have been carried out by introduction of non-metals, such as carbon, nitrogen, sulfur, fluorine, iodine and boron into the TiO_2 bulk to successfully cause the red shift of the absorption onset of TiO_2 to the visible region and enhance the photocatalytic activity.

Besides nonmetal doped TiO_2 systems, metals for example, Ag, Pt, Fe, W, La, Eu and Zn are another kind of efficient dopant which can facilitate to separate the photogenerated electron–hole pairs resulting in enhancement of photocatalytic activity for both oxidation and reduction.

Studies suggested that the incorporation of Zn^{2+} to TiO_2 host led to a significant increase of photoelectric properties (Mohammadi & Fray, 2010; Niaki, Bakhshayesh, & Mohammadi, 2014; D. Zhang, 2012; Y. Zhang et al., 2011). Since, a number of valence electrons of Zn^{2+} is lower than Ti^{4+}, the excess of hole can create an accepter band near that of the TiO_2. Y. Zhang (2012) had recently fabricated the Zn-doped TiO_2 layer (with Zn = 0-1%) served as a photoanode. They revealed that the slightly doping content of Zn (0.5-1%) ion can promote the increasing photoelectron concentrations and also separation of the photo-generated charge as well as restrain the recombinations. Niaki(2014).

3.2 Methods of Nanoparticle Synthesis

Nanoparticles with given size and characteristics are required in nanotechnology. Nanoparticles growth mechanism determines distribution function of nanoparticles on size, physical-chemical properties of nanoparticles medium and etc. Because of, known of growth mechanism give possibility control of preparation of nanoparticles and to obtain nanoparticles with given parameters (mean diameter, standard deviation, coefficient polydispersity and other) and characteristics (magnetic moment). Nanoparticles growth mechanism is enough complex process and depended from many conditions (temperature, viscosity, concentration of medium and etc.). Conditions determinant of nanoparticle growth are changed in the dependence on method preparation of nanoparticles (Rajput, 2015). Nanoparticles (NPs) with good and controlled quality are desirable for their commercialization in various fields of applications. There are two basic approaches commonly employed to prepare NPs; (1) top-down approach, where synthesis is initialized with the bulk counterpart that leaches out systematically leading to the generation of fine NPs. Photolithography, electron beam lithography, milling techniques, anodization, ion and plasma etching are some of the commonly used top-down methods for the mass production of NPs; (2) bottom-up approach, which involves the coalescence or assembling of atoms and molecules to generate diverse range of NPs. Examples of bottom-up approach include self-assembly of monomer/polymer molecules, chemical or electrochemical nanostructural precipitation, sol–gel processing, laser pyrolysis, chemical vapour deposition (CVD), plasma or flame spraying synthesis and bio-assisted synthesis. In general, NP synthesis methods can be divided in three groups:

(1) physical methods,
(2) chemical methods, and
(3) bio-assisted methods.

3.2.1 Physical Methods for the Synthesis of Nanoparticles

Physical methods apply mechanical pressure, high energy radiations, thermal energy or electrical energy to cause material abrasion, melting, evaporation or condensation to generate NPs. These methods mainly operate on top-down strategy and are advantageous as they are free of solvent contamination and produce uniform monodisperse NPs. At the same time, the abundant waste produced during the synthesis makes physical processes less economical. Mechanical milling, laser ablation, electrospraying, inert gas condensation, physical vapour deposition, laser pyrolysis, flash spray pyrolysis, melt mixing are some of the most commonly used physical methods to generate NPs (Dhand et al., 2015) (Yadav, Yadav, & Singh, 2012).

The mechanical alloying/milling process was originally developed by Benjamin of the International Nickel Company for the production of oxide dispersion strengthened (ODS) super alloys(Benjamin, 1970). During the process, raw powder particles with a size of several microns experience severe plastic deformation, i.e. undergo a repetitive cold welding and fracturing mechanism (Koch, 1993). The kinetics of mechanical milling or alloying depends on the energy transferred to the powder from the balls during milling (S. Tjong & Chen, 2004). The energy transfer is governed by many parameters such as the type of mill, the powder supplied to drive the milling chamber, milling speed, size and size distribution of the balls, dry or wet milling, temperature of milling and the duration of milling (Yadav et al., 2012).

Mechanical alloying (MA) is now recognized as a versatile process for the fabrication of a broad range of nanocrystalline powders. These powders include ODS alloys (Schwarz & Johnson, 1983), amorphous alloys (Hellstern, Fecht, Fu, & Johnson, 1989; Shen et al., 1995), nanocrystalline metals/alloys (Hellstern et al., 1989) and supersaturated solid solution (B.-L. Huang, Perez, Lavernia, & Luton, 1996; Shen & Koch, 1996). The disadvantage of ball-milling for making nanocrystalline powders is the contamination of products from the milling media (balls and vial) and atmosphere. (Shen & Koch, 1996).

Physical vapor deposition (PVD) is a versatile synthesis method and capable of preparing thin film materials with structural control at the atomic or nanometer scale by careful monitoring the processing conditions. PVD involves the generation of vapor phase species either via evaporation, sputtering, laser ablation or ion beam. In evaporation, atoms are removed from the source by thermal or electron means; in sputtering, atoms are ejected from the target surface by the impact of energetic ions. In the former case, the vapor phase species that experience collisions and ionization are condensed onto a substrate follow by the nucleation and growth. Thermal evaporation has a limitation in multi component materials since one of the metallic elements typically evaporates before the other due to the differences in vapor pressures of the evaporating species. On the contrary, sputtering is capable of depositing high melting point materials such as refractory metals and ceramics, which are difficult to fabricate using evaporation. Since the sputtered atoms carry more energy than the evaporated atoms, the sputter-grown films usually have higher density .Owing to the lower purity of the sputtering target materials, sputtered films are more prone to contamination than evaporated films(S. Tjong & Chen, 2004).

Flame spray pyrolysis (FSP). FSP is the latest of all the flame aerosol technologies. It is a one-step combustion process where the precursor is in liquid form, with significantly higher combustion enthalpy (>50% of total energy of combustion), usually in an organic solvent. The important technological elements of this process include self-sustaining flame, usage of liquid feeds and less volatile precursors, proven scalability, high temperature flames and large temperature gradients. It is one of the most exploited techniques for the production of complex and functional NPs. For the formation of particles, the liquid precursor can follow the droplet-to-particle route or gas-to-particle route; however, later results in more homogenous morphologies and size. For NPs fabrication, precursor spray has to follow the sequential steps; (1) precursors evaporate/decompose forming metal vapors; (2) nucleation as a result of supersaturation; (3) growth by coalescence and sintering; and (4) particle aggregation (by chemical bonds) and agglomeration (by physical interactions) (Dhand et al., 2015).

Melt mixing. method involves the mechanical mixing of a polymer with modified nanofillers by extrusion or kneading, and less commonly by injection moulding technique. This is one of the oldest methods to design polymer composites with NPs as the fillers to achieve desired material characteristics. This is the most commonly used mechanical process because it is environment friendly and it is also well suited for current industrial practices (Dhand et al., 2015).

3. 2. 2 Chemical Methods for the Synthesis of Nanoparticles

Sol-gel method, microemulsion technique, hydrothermal synthesis, polyol synthesis, chemical vapour synthesis and plasma enhanced chemical vapour deposition technique are some of the most commonly used chemical methods for the NPs synthesis (Dhand et al., 2015).

Chemical vapour deposition (CVD) is a process, which is often used for the deposition of solid films from vapour phase via chemical reactions occurring at very high temperature condition. Thin films produced by CVD process at certain conditions also contain ultra fine particles. The main steps that occur in the CVD process can be summarized as:

(a) Transport of reacting gaseous species to the surface.
(b) Adsorption of the species on the surface.
(c) Heterogeneous surface reaction catalyzed by the surface.
(d) Surface diffusion of the species to growth sites.
(e) Nucleation and growth of the film.
(f) Desorption of gaseous reaction products and transport of reaction products away from the surface (Hitchman & Jensen, 1993; Sherman, 1987)

CVD is a more complex method than PVD. CVD exhibits several distinct advantages such as the capability of producing highly pure and dense films or fine particles at reasonably high deposition rates, and the capablility of coating complex-shaped components uniformly due to its non-line-of-sight nature. CVD is widely used

for the deposition of metallic, ceramic and semiconducting thin films. Depending on the activation sources for the chemical reactions, the deposition process can be categorized into thermally activated, laser-assisted and plasma-assisted CVD(Hitchman & Jensen, 1993; Sherman, 1987).

Plasma enhanced chemical vapour deposition (PECVD). Plasma enhanced chemical vapour deposition, also called as plasma assisted chemical vapour deposition (PACVD), is a popular CVD process which is widely used for the deposition of thin films. PECVD process can also be used for the synthesis of NPs. As the name suggests, plasma enhances the chemical reactions for the synthesis of thin films and NPs. PECVD unit mainly includes: (1) vacuum processing system, (2) gaseous precursors, (3) power supply (AC or DC) and (4) heater. Unlike usual CVD process, the synthesis of thin films and NPs by PECVD takes place at comparatively lower temperature. As the plasma is partially ionized gas, ionized species and radicals participate in growth of thin films and NPs (Dhand et al., 2015).

Polyol synthesis. Polyol process is the synthesis of metal-containing compounds using poly (ethylene glycol)s as the reaction medium, that plays a role of solvent, reducing agent and complexing agent at the same time, with dissolved stabilizing/protecting agents. This chemical process was used to synthesize a wide range of metal based NPs (Ag, Pt, Pd, Pr,Cu), metal oxide NPs (ZnO, indium-tin-oxide; ITO, Gd_2O_3, Cu_2O), magnetic NPs and metal hybrid NPs (Dhand et al., 2015).

The sol–gel process in general is based on the transition of a system from a liquid "sol" (mostly a colloidal suspension of particles) into a gelatinous network "gel" phase. With this, it is possible to create at low temperature ceramic or glass materials in a wide variety of forms. It is a long-established industrial process that is very cost-effective and versatile (Daraio & Jin, 2012; Dhand et al., 2015). The sol–gel method was used for the fabrication of ceramics, monolithic glasses, submicron particles, and aerogel materials, at a relatively low temperature. It has been used to synthesize nanoparticles in colloidal and film form for decades(C. J. Brinker & Scherer, 2013; De Jonghe & Rahaman, 2003; Schmidt, 2010).

In acid solution, the sol-to-gel transition allows the solid phase to be shaped into films, fibers and monoliths. For preparing coating films and fibers, the sol must exhibit spinnability. It appears that only solutions containing long-chained polymers are spinnable. Films are generally coated on the surface of the substrate via spin-coating and dipping processes. Gel fibers are made by fiberdrawing from the viscous alkoxide solution at or near room temperature. The flow chart of sol–gel processing is schematically shown in Figure 3.1 (Pierre, 1998). In contrast, a colloidal sol is generated upon basic hydrolysis of metal alkoxides(C. Brinker, Keefer, Schaefer, & Ashley, 1982; C. J. Brinker & Scherer, 2013). The gel is colloidal when the solid network is made of round sol particles.

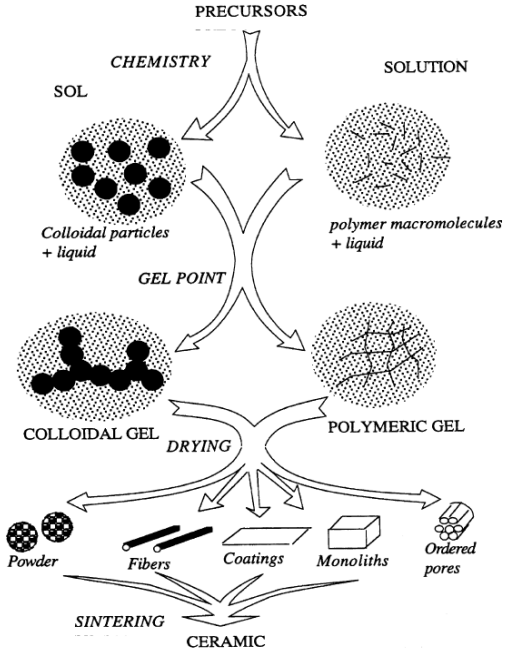

Figure 3. 1 Flow chart of so-gel processes (Daraio & Jin, 2012)

3.2.2.1 Steps Involved in Sol-Gel Process

Mixing: In this part of this method, a colloidal solution is formed via mechanical mixing of colloidal particles in water as a solvent at a precipitation preventing pH. The metal alkoxide precursor M(OR)4 reacts with water and undergoes hydrolysis and polycondensation reactions, the formation of a colloidal dispersion of extremely small particles (1–2 nm) takes place that finally converts into a 3-D network of the corresponding inorganic oxide (A. Kumar et al., 2015).

In this process, reactive metal precursors were initially hydrolized, followed by condensation and polymerization reactions. Metal alkoxides are metalorganic compounds having an organic ligand attached to a metal or metalloic atom. They are the result of direct or indirect reactions between a metal M and an alcohol ROH. Typical examples are methoxide (OMe; $MOCH_3$) and ethoxide (OE_t; MOC_2H_5). During hydrolysis, the alkoxy groups (OR) are replaced by hydroxo ligands (OH), i.e (Figure 3.2).

$$M(OR)_z + H_2O \rightarrow M(OH)(OR)_{z-1} + ROH \quad (3.1)$$

Where R is an alkyl group, C_nH_{2n+1}. The mechanism of this reaction involves the addition of a negatively charged $HO^{\delta-}$ group to the positively charged metal center ($M^{\delta+)}$followed by the removal of ROH(C. J. Brinker & Scherer, 2013; Pierre, 1998):

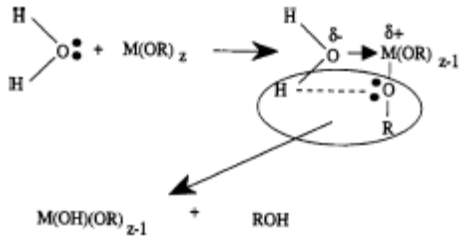

Figure 3. 2 Schematic Illustration of the mechanism of solgel reaction

Several factors are known to affect the hydrolysis reaction(C. J. Brinker & Scherer, 2013; Yoldas, 1986). These include:

(a) The nature of the alkyl group.
(b) The nature of the solvent.
(c) The concentration of each specie in the solvent.
(d) The temperature.
(e) The water to alkoxide molar ratio.
(f) The presence of acid or base catalysts.

Subsequent condensation eliminates either water or alcohol to produce metal oxide or hydroxide linkages. In this process, two mononuclear complexes of M, each

comprising only one metal M, can react with one another to form a polynuclear complex consisting of two metal atoms. Condensation occurs only when at least one hydroxo ligand is bonded to the cation M, and is designated as M-OH for simplicity. Condensation can proceed via olation and oxolation reactions. Olation is a reaction by which hydroxo or ‘‘ol’’ bridge M–OH–M bond is formed between two cations whilst oxalation involves the formation of oxo bridges M–O–M between to metal cations M(C. J. Brinker & Scherer, 2013):

$$\text{Olation : M-OH+M-OH}_2 \rightarrow \text{M-OH+H}_2\text{O}$$
$$\text{Oxalation : M-OH + H - OM} \rightarrow \text{M-O-M+H}_2\text{O}$$
$$\text{M-OH + ROM} \rightarrow \text{M-O-M+ROH} \qquad (3.2)$$

The ‘‘ol’’ or ‘‘oxo’’ bridges between two metal atoms lead to the formation of condensed oxide or hydroxide species. Under acid conditions, three-dimensional solid phase networks consisting of extended linear M–O–M chain polymers are developed (C. Brinker et al., 1984). Inorganic polymerization is believed to occur in three stages during acid-catalyzed condensation (Iler, 1979):

(i) Polymerization of monomer units to form particles.

(ii) Growth of particles.

(iii) Linking of particles into chains, then solid networks that extend throughout the liquid medium, thickening it to a gel.

Gelation: As process takes place, three-dimensional networks start forming from colloidal particles and condensed silica. The size of the particles and the gelation process decides the properties of the gel. In the gelation process, there is a subsequent increase in the viscosity and this will result in the shape of casting container. Over the time, with controlled change in viscosity, fibers are spun together while the gelation occurs. Gelation results into agglomeration with colloidal particle which is due to interactions among the components which can be electrical in nature (A. Kumar et al., 2015).

Aging: This part of sol-gel process is also called Syneresis. It includes the maintenance of the cast object for a period which can vary from hours to days. During the aging process, polycondensation continues along with solution it is immersed in and the gel-network will reprecipitate. This process will increase the thickness of interparticle necks and decrease the porosity. Hence, the potency of the gel increases with this and produces a product which is resistive to cracking while drying (A. Kumar et al., 2015).

Drying: In the drying process, excess of solvent is removed from the complex network. Removal of the solvents and appropriate drying are important steps to achieve gel densification. When a solvent is evaporated from the gel under atmospheric conditions, capillary pressure due to the interfacial tension of the solvent develops a high stress on the gel network. This leads to considerable shrinkage and fracture of the gel during drying. The resultant hard, glassy and porous product is called a xerogel. In the case where the liquid within the gel is removed above its critical temperature and pressure (hypercritical) in an autoclave, the capillary pressure can be eliminated. The product thus obtained is referred to as an aerogel (Teichner, Nicolaon, Vicarini, & Gardes, 1976; Utamapanya, Klabunde, & Schlup, 1991). Aerogel is generally armorphous and exhibits several unique properties such as high surface areas and high porosities, low densities, and low conductivities(Fricke & Reichenauer, 1987).

Densification: The gel produced is heated at elevated temperatures which will cause densification of the gel. This will also eliminate the pores in the gel and makes the density approximately around fused quartz or silica. The temperature of densification depends on the pore dimension, pore connectivity and its surface area (A. Kumar et al., 2015).

A large variety of parameters affecting the sol-gel process, such as type of solvent, timing, pH, precursor, water/metal ratio, etc., alllow a versatile control of structural and chemical properties of the final oxide materials (Camargo, Satyanarayana, & Wypych, 2009).

The aqueous sol–gel process provides an economical advantage with minimum environmental impact.Indeed, solgel processing has several attributes (Bensebaa, 2012):

a. efficient and cost-effective process to produce NPs and films;

b. most materials can be obtained at low temperatures;

c. possibility of greater control over material chemistry and homogeneity;

d. sol-gel powders can be consolidated at much lower pressures and temperatures;

e. high-density materials without the need for low-temperature binders;

f. thermomechanical processing of films and materials can be accomplished at significantly lower processing conditions;

g. uniform infiltration is achievable because of the continuous 3D structure of the sol-gel-based nanoparticle system.

3.2.3 Bio-assisted Methods for the Synthesis of Nanoparticles

Bio-assisted methods, biosynthesis or green synthesis provides an environmentally benign, low-toxic, cost-effective and efficient protocol to synthesize and fabricate NPs. These methods employ biological systems like bacteria, fungi, viruses, yeast, actinomycetes, plant extracts, etc. for the synthesis of metal and metal oxide NPs. Bio-assisted methods can be broadly divided into three categories:

(i) Biogenic synthesis using microorganisms

(ii) Biogenic synthesis using biomolecules as the templates

(iii) Biogenic synthesis using plant extracts (Dhand et al., 2015).

CHAPTER FOUR
NANOCOMPOSITE COATINGS

4.1 General Information

Many conventional and advanced technological applications demand materials with well-defined surface properties, fulfilling specific requirements, which aim at both valorising the material and advancing the related technology. Nowadays, the advances in surface engineering, nanotechnology and nanomaterials allow the manipulation of materials' composition down to the molecular scale, paving the way for new Hi-Tech functional materials. The surfaces of many materials can be functionalized by applying coatings (Y. X. Gan, 2012).

A nanocomposite coating is a coating with a nanocomposite structure. This means that it is composed of two or more immiscible phases, of which at least one is restricted to the nanometer scale in at least one dimension. Therefore, a nanocomposite coating is formed by a matrix where filler nanostructures are dispersed (Martínez-Martínez, 2013).

The properties of a nanocomposite coating depend on the chemical nature of their phases, their relative proportion, and the size of the filler. These properties do not necessarily follow the rule of mixture (i.e., certain properties of a nanocomposite can be improved with respect to those of each component alone). This kind of synergic effect is obtained by a proper control of the structure of the nanocomposite (Martínez-Martínez, 2013). Nanocomposite materials can be classified into three main categories according to their matrix materials i.e. ceramic matrix nanocomposites (CMNC); metal matrix nanocomposites (MMNC) and polymer matrix nanocomposites (PMNC) (Y. X. Gan, 2012). Different types of nanocompocites are shown in Table 4.1 (Camargo et al., 2009).

Table 4. 1 Different types of nanocomposites

Class	Examples
Metal	Fe-Cr/Al_2O_3, Ni/Al_2O_3, Co/Cr, Fe/MgO, Al/CNT, Mg/CNT
Ceramic	Al_2O_3/SiO_2, SiO_2/Ni, Al_2O_3/TiO_2, Al_2O_3/S.C, Al_2O_3/CNT
Polymer	Thermoplastic/thermoset polymer/layered silicates, polyester/TiO_2, polymer/CNT, polymer/layered double hydroxides.

There are two types of nanocomposite coatings: (i) matrix-reinforced, where the reinforcing phase is within nanoscale, and (ii) layered coatings, where the thickness of individual layers are within nanoscale dimensions; Figure 4.1.

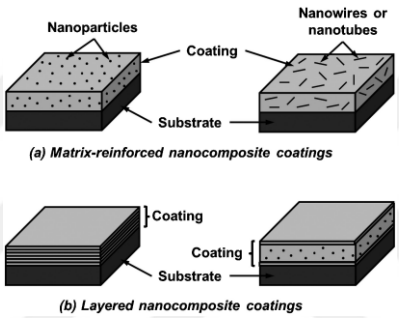

Figure 4. 1 Schematics of nanocomposite coatings (J. A. Gan & Berndt, 2015)

Despite their nano dimensions, most of the processing techniques of the three types of nanocomposites remain almost the same as in microcomposites.

4.2 Classification of Nanomaterials

4.2.1 Ceramic Matrix Nanocomposites (CMNC)

Many methods have been described for the preparation of ceramic matrix nanocomposites. The most common methodologies, as used for microcomposites, are Conventional powder method; Polymer precursor route; Spray pyrolysis; Vapour techniques (CVD and PVD), and Chemical methods, which include the sol-gel process, colloidal and precipitation approaches and the template synthesis (Camargo et al., 2009).

4.2.2 Polymer Matrix Nanocomposites (PMNC)

Many methods have been described for the preparation of polymer nanocomposites, including layered materials and those containing CNTs. The most important ones are i) Intercalation of the polymer or pre-polymer from solution; ii) In-situ intercalative polymerization; iii) Melt intercalation; iv) Direct mixture of polymer and particulates; v) Template synthesis; vi) In-situ polymerization; and vii) Sol-gel process. Publications dealing with various methods for the incorporation of nanodispersoids into conducting polymers are also available; the most prominent one is probably the incorporation of inorganic building blocks in organic polymers (Camargo et al., 2009).

4.2.3 Metal Matrix Nanocomposites (MMNC)

The most common techniques for the processing of metal matrix nanocomposites are Spray pyrolysis; Liquid metal infiltration; Rapid solidification; Vapour techniques (PVD, CVD); Electrodeposition and Chemical methods, which include colloidal and sol-gel processes (Camargo et al., 2009).

4.3 Processing Methods of Nanocomposites

4.3.1 Vapour Technologies

Nanostructure and particularly nanocomposite coatings deposited by physical vapour deposition or chemical vapour deposition, have gained considerable attention due to their unique physical and chemical properties, e.g. extremely high indentation hardness (40-80 GPa), corrosion resistance, excellent high temperature oxidization resistance, as well high abrasion and erosion. Different techniques are available for the preparation of nanocomposite coatings. The most promising methods are plasma assisted chemical vapour deposition (PACVD), thermally induced chemical vapour deposition (TCVD), magnetron sputtering, vacuum arc evaporation, laser ablation and hybrid techniques consisting of a combination of these. Other techniques, such as ion beam deposition, electrodeposition are also used (Table 4.2) (Lukaszkowicz, 2011).

Table 4. 2 Main preparation methods for nanocomposite thin films (S. Zhang, Sun, & Bui, 2007)

Group	Sub-group	Methods
Physical vapour deposition (PVD)	Thermal evaporation (TE)	Pulsed laser deposition (PLD) Electron beam deposition (EB-PVD)
	Sputter deposition	Magnetron sputtering Ion beam sputtering
	Arc vapour deposition	Vacuum arc deposition Filtered arc deposition
	Ion implantation	Ion beam deposition (IBD)
Chemical vapour deposition (CVD)		Plasma enhanced CVD (PECVD) Plasma assistant CVD (PACVD) Electron cyclotron resonance CVD ((ECR-CVD)

Uniform deposition for complicated geometries and high deposition rate are the advantages of the CVD method. However, the main concern for the CVD process is that the precursor gases, $TiCl_4$, $SiCl_4$ or SiH_4, may pose problems in deposition because they are a fire hazard and corrosive. In conventional thermally activated CVD heating provides sufficient high temperature for the dissociation of gaseous species (Lukaszkowicz, 2011).

For most applications (e.g. highspeed steel, hot work tool steel, etc.) the low deposition temperature is required to prevent substrate distortion and loss of mechanical properties. It precludes the use of substrates having melting points or tempering temperature much lower than the reaction temperature. Plasma assisted CVD exhibit a distinct advantages over thermal CVD owing to its lower deposition temperature (Lukaszkowicz, 2011).

Vacuum arc evaporation technology has high ionization (≥90 %) but limited material. Magnetron sputtering is a low temperature technology, which can deposit various materials, but its ionization is low. In magnetron sputtering process the

energetic ion (several hundred to a few thousand electronovolts) bombardment is used to vaporize the target. During magnetron sputtering process, the sputtered atoms carry more energy than the evaporated atoms, therefore sputter-grown films usually have higher density. Moreover, ion bombardment of the growing film can restrict the grain growth and permit the formation of nanocrystalline. In arc evaporation process atoms are removed from source by thermal or electron means. Thermal evaporation has a limitation in multicomponent materials since one of the metallic elements typically evaporates before the other. The advantages of deposition of coatings by means of vacuum arc are the high deposition rate and fully ionized plasma. The disadvantages are the emission of droplets of molten metal from the cathodic spot and the uncontrolled movement of the cathodic spot over the surface (Lukaszkowicz, 2011).

In this process, both porous and dense layers can be obtained by varying process parameters, such as temperature (Beckel et al., 2007). Moreover, the surface morphology of the deposited layer can be easily tailored by varying deposition conditions (Beckel et al., 2007). However, this process requires high-cost equipment and exhibits low deposition rates of a few nanometers per minute results.

4.3.2 Sol-Gel Method

Extensive work is carried out to prepare better quality of nanostructures using the sol-gel process (S.-I. Kim, Lee, Ahn, Song, & Jang, 2013) in order to achieve good electrochemical properties. The sol-gel method can be termed as the conversion of a precursor solution into an inorganic solid by chemical route. It is well known that the sol-gel method is simple and cheap, and it provides products of high purity and good homogeneity. In this method, the surfactants, solvents, reaction time and temperature are the main factors to obtain suitable structures with remarkable electrochemical performance. It mainly consists of the following four steps - (i) preparation of the precursor solutions, (ii) formation of the intermediates sol, (iii) conversion from sol to gel and (iv) calcination(Sk, Yue, Ghosh, & Jena, 2016).

4.4 Electrodeposition

Electrodeposition is a fabrication method of these nanostructured coatings with highly desirable fabrication process and outstanding functional and mechanical characteristics of produced coatings (Nasirpouri, 2017).

Electrodeposition method is an economical and versatile technique compared to other preparation techniques. Moreover, it is quickly scaled up to industrial production, offering an inexpensive method to produce large area samples. These are some of the reasons that make this method so popular. In addition, the low processing temperature (around room temperature) minimizes interdiffusion or chemical reaction between the substrate and coating species. The film thickness can be accurately controlled by monitoring the consumed charge and the composition can be tailored by the electrical applied profile and bath composition (Bicelli et al., 2008). The occlusion electrodeposition, or electrochemically co-deposition method, where the particles incorporation occurs simultaneously with the metal ions reduction, uses a precursor bath loaded with the particles to be occluded (S. C. Tjong, 2007).

This technique is widely used to obtain metal matrix composites due to its ease of preparation, low cost and versatility. The concentration of particles suspended in solution varies from 2 up to 200 g/L producing composites with typically 1-10 vol.% of embedded particles. With the increasing availability of nanoparticles, the interest of the low-cost and lowtemperature composite electroplating is continuously growing, with the major challenge being the achievement of high co-deposition rates and homogenous distribution of the particles in the metallic matrix (S. C. Tjong, 2007).

Fundamentally, the electrocodeposition process and hence the structure, the morphology and the properties of the composite coatings is affected by the electrodeposition parameters like the electrolysis conditions (composition and agitation of the electrolytic bath, presence of additives, temperature, pH), the electrical profile and the particle properties (type, size, shape, surface charge, concentration and dispersion (S. C. Tjong, 2007).

Some studies have proposed model behaviour for the co-electrodeposition process. Guglielmi explained the peculiarities of the co-deposition of inert particles from electrolytic solution by a mechanism based on two successive adsorption steps. In the first step, the particles are loosely adsorbed, and they are in equilibrium with the particles in suspension. This adsorption has a physical natüre in which the particles surrounded with a thin layer of electrolyte ions or solvent molecules (particle-ion complex molecules) move towards the electrode surface. They reside to the Helmholtz layer and then weakly adsorb into the cathode surface. The surrounding layer formed around the particles prevents any direct contact and interaction with the electrode surface. Thus, they remain in this loosely bonded situation until the next step. In the second step the particles are irreversibly adsorbed. This step has an electrochemical nature. At this stage under the effect of the electrical field around the cathode, a charge transfer reaction occurs between the metal ions and the cathode surface. This removes the surrounding layer around the particles making them well incorporated into the metal deposit. The strong adsorption occurring in the second step depends on the electrode potential. One particular feature of this model is that the particle load in the electrodeposit increases with the particle concentration in solution as well as with the deposition current density. However, the increasing rate of particle content in the electrodeposit is impaired at higher concentration of particles and higher current densities. This limits the incorporation magnitude or the fraction of particle in the co-deposit up to a certain value likely owing to the saturation of the cathode surface by the particles. Forming a dense layer of particles on the surface of the cathode through the electrolyte prevents absorbing of further particles. Guglielmi's model did not consider the hydrodynamic effects and the influence of particle size. These made some deficiencies of this model for interpreting the co-depositing mechanisms (Guglielmi, 1972).

The transport of nanometer size particles to the growing surface is controlled by convective diffusion as predicted by Celis et al. model. They showed that the kinetics of nanometer size particle incorporation into a growing film depends on the residence time at the surface. The model is valid if the diffusion layer thickness for particles is considerably smaller than the diffusion layer thickness for ions in solution due to the

difference in diffusion coefficients and for the particle sizes smaller than the diffusion layer thickness. To simplify the models presented, a five step generally admitted co-deposition mechanism has been deduced which include: (1) formation of ionic clouds on the particles, (2) convection towards the cathode, (3) diffusion through a hydrodynamic boundary layer, (4) diffusion through a concentration boundary layer and finally, (5) adsorption at the cathode where particles are entrapped within the metal deposit. Figure 4.2 schematically shows the steps mentioned in this model (Guglielmi, 1972). C.T.J. Low, R.G.A. Wills, F.C. Walsh, Surface Coatings Technology 201, 371–383 (2006

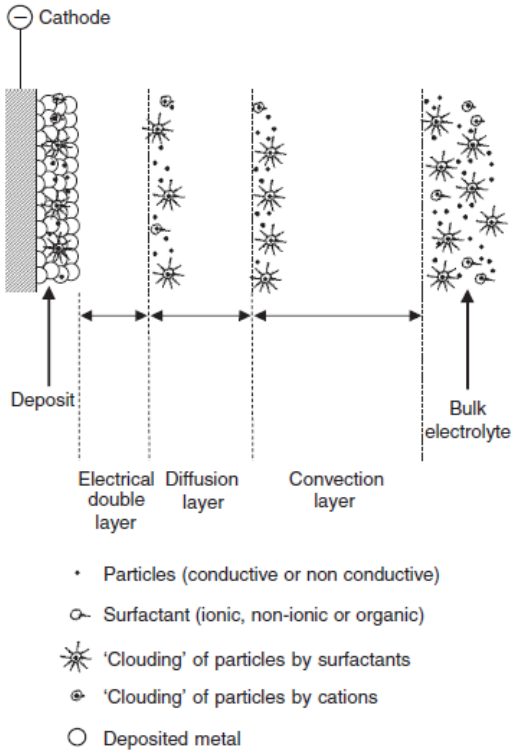

Figure 4. 2 Mechanisms of particle codeposition into a metal deposit (Roos, Celis, Fransaer, & Buelens, 1990).

It can be categorized the co-electrodeposition parameters into electrodeposition technique, particle properties and electroplating bath parameters. Electrodeposition techniques are basically divided into potentiostatic and galvanostatic. For co-electrodeposition techniques, the galvanostatic techniques have been mainly used. Three different techniques used for co-electrodeposition of metal matrix nanocomposite coatings are direct current (DC), pulse current (PC) and reverse pulse

current (PRC). Electrolyte bath parameters include electrolyte concentration, additives, temperature, pH, surfactant type and concentration, hydrodynamics (laminar, mixed, turbulent regimes) and electrode geometry and configuration (rotating disk electrode, rotating cylinder electrode, plate-in-tanks, parallel plate electrodes, sediment co-electrodeposition and many variations).

4.5 Process Paarameters of Electrochemical Deposition Method

4.5.1 Effect of Current Density

In many studies, DC technique is used as the most common method of co-electrodeposition of nanocomposite coatings exhibiting desirable properties. This technique is based on the concept that the incorporation of nanoparticles occurs simultaneously with the reduction reaction of an ionic species to form the metal surface. PC and PRC techniques have been more recently paid much attention owing to their ability to produce more efficient incorporation of higher concentrations of nanoparticles as well as a wider range of deposit compositions and properties. The PC technique is based on alternating two or more direct cathodic currents for various deposition times whereas PRC technique has similar characteristics but combines a cathodic current and an anodic current along with off times between each pulse. The methods have been the most successful for embedding higher concentrations of nanoparticles. One reason would be the elimination a fraction of the electrodeposited metal during the off time. In PRC, the anodic pulse even dissolves more metal deposited during the cathodic on pulse (Nasirpouri, 2017).

Generally, the amount of particles incorporation in the metal matrix is enhanced by increasing of the current density up to a limit and beyond this value the nanoparticles content in the coating decreased. It was suggested that the particles adsorbed cations moved directly to the cathode under the effect of gravitational force and electronic force then captured by the growing metals. At low current densities the rate of transfer of particles is faster than the growth rate of the metal. On the other hand, at higher current densities the situation is reversed so the particle content in the composite coating decreases (C. Wang et al., 2008)

4.5.2 Effect of Particle Characteristics

The most important properties of particles in co-electrodeposition of metal-matrix nanocomposites may be but not limited to particle load or concentration in the electrolyte solution, surface charge and surface physics and chemistry, type and material nature, shape and morphology and size. These of characteristics interplay with other to define the amount of nanoparticles in electrolyte solution. This in turn would significantly affect the volume fraction of particles in the metal matrix (Nasirpouri, 2017).

The size of particles will affect the co-electrodeposition mechanism. In one hand, it changes the rate of incorporation into the metal deposit. Findings have suggested that as the size of nanoparticles becomes smaller, more can be incorporated into a metal deposit per unit volume. The size of particles changes the mechanism of mass transport of particles from diffusion-convection for finer particles to diffusion-gravitational for larger particles (Shao, Vereecken, Cammarata, & Searson, 2002). In the other hand, the presence of nanosized particles in a metal deposit may change the nucleation rate of metal deposit towards finer grain metal matrices (Nasirpouri, 2017).

4.5.3 Electrolyte Parameters

4.5.3.1 Agglomeration Control

One major phenomenon is the monodispersion of particles in an electrolyte. Nanoparticles with a very high surface energy tend to easily agglomerate in highly conductive metal electrolytes. This lowers the uniform distribution of the particles. The particles must be well dispersed in the electrolyte by utilizing effective mixing methods (Nasirpouri, 2017).

The agglomeration of particles in the plating bath can also be reduced by ultrasonic energy treatment. The propagation of ultrasound waves in the solution generates large pressure causing stress that destroy the binding energy between particles. Kuo et al(Kuo, Chen, Ger, & Hwu, 2004) studied the effect of ultrasound energy on the

electrocodeposition of Ni-alumina composite coating. They reported that the diameter of the agglomerated alumina particles could be reduced by applying ultrasound energy but the resulting dispersion is limited which led to low alumina content within the composite coating. The alumina content can be increased by decreasing the concentration of Ni^{2+} ions in the plating bath (Ahmad & Mohamed, 2014).

4.5.3.2 Surfactants

A combination of cationic, anionic and non-ionic surfactants can be used to achieve control of surface charge on the particles and the degree of suspension in the electrolyte (Nasirpouri, 2017).

It was reported by many researchers that addition of a cationic surfactant increases the particle co-deposition in the metal matrix(Pompei, Magagnin, Lecis, & Cavallotti, 2009; L. Wang, 2008). The enhancement of particle codeposition into metal matrix is associated with the modifications take place on the particle surface caused by adsorbed ions or surfactant molecules. This adsorption promotes the electrophoretic migration of the particle towards cathode but this effect is more pronounced if the particle size is in nanoscale (Rudnik, Burzyńska, Dolasiński, & Misiak, 2010). The cationic surfactant can adsorb on the particle surface developing a net positive charge on its surface so increasing their affinity towards cathode and hence increases the stability of particles suspension and prevents agglomeration. In this way it is believed that cationic surfactant enhances the incorporation of particles in the metal matrix. However, the extent of particles co-deposition depends on the type of surfactant (Ahmad & Mohamed, 2014).

4.5.3.3 Particle Concentration

Another parameter related with the electrolyte is the particle load or concentration in the electrolyte. The effect of nanoparticle concentration in the electrolyte on their concentration in the metal deposit has been predicted to follow a Langmuir isotherm

adsorption phenomenon. Two general observations can be made: (1) the volume fraction of nanoparticles in the metal deposit increases substantially when the amount of nanoparticles concentration in the solution increases and (2) a saturation state of particles in the deposit is reached at high nanoparticle concentration in the solution (Nasirpouri, 2017).

The dependence of particle content in the deposit and consequently the microstructure and coat properties on the particle content in the plating bath was studied by many authors (Bapu & Jayakrishnan, 2012; D. K. Singh & Singh, 2012).

4.5.3.4 Electrolyte Agitation

Influence of bath agitation and cathode movement have been vigorously investigated as it is normally carried out for two purposes, namely to keep the particles suspended in the electrolyte and to transport the particles to the cathode surface. Many investigations have found that increased agitation generally enhances the amount of particles in the metal deposit. However, excessive agitation may lead to a lower quantity of particles in the metal deposit. This may be explained by vigorous hydrodynamic forces in the electrolyte removing the particles from the cathode surface before they can be entrapped in the metal deposit (Nasirpouri, 2017).

The rate of stirring affects the co-deposition has two contradictory ways i.e. (i) increasing the rate of agitation leads to increase the content of particles in the nanocomposites , (ii) at high rates of agitation the particle nanocomposites content decreases (Hovestad & Janssen, 1995).

4.5.3.5 Electrolyte Temperature

The effect of temperature of electrolyte on the co-electrodeposition of nanocomposites is also quite important. A similar result is observed by Kim and Yoo. At higher temperatures it is in accordance with the Langmuir adsorption theory that the adsorption of the particulates is degraded. This decreases the overpotential of the

cathode and the electric field and as a result SiC particles are hardly embedded in the Ni metal matrix (Nasirpouri, 2017) (S. K. Kim & Yoo, 1998).

The effect of temperature on the percent of SiC codeposition into Ni matrix was studied by Vaezi et al (Vaezi et al., 2008). Their results showed that the percent of codeposited SiC nanoparticles increases with temperature of the plating bath up to 50 ºC. This behavior was attributed to increase of activity of SiC particles with temperature. However, at higher temperatures the cathode overpotential decreased and hence the adsorpability of the particulates which decreased the percent of their incorporation in the metal matrix. As the temperature increases, the thermodynamic driving force of crystallization decreases with an increase in the critical size of the nucleus resulting to lower nucleus densities i.e. formation of coarse grain (Natter & Hempelmann, 2008; Turner, 1953). On the other hand, the increase in temperature leads to increase in the kinetic driving force which leads to increase in the rate of nucleation and subsequent formation of fine grains (Rashidi & Amadeh, 2009). Hence, it was concluded that below 45 ºC the kinetic driving force is the dominant factor in determining the crystallite size, whereas above 45 ºC the thermodynamic driving force is the controlling factor of the nucleation rate.

CHAPTER FIVE
EXPERIMENTAL STUDIES

Thesis was composed of two main parts in terms of production and characterization of the samples. First, TiO_2 and Zn doped TiO_2 nanoparticles were synthesized by sol-gel method. Then Ni-TiO_2 and Ni-Zn/TiO_2 nanocomposite coatings were deposited by electrodepositon technique. Applied current density (3, 5 and 7 $A.dm^{-2}$) was selected as a paramaters during deposition.

5.1 Production of Nanoparticles

TiO_2 and Zn doped TiO_2 nanoparticles were synthesized by sol-gel method. For the preparation of TiO_2 nanoparticles, the materials used were titanium tetra-isopropoxide [$Ti(OC_3H_7)_4$], citric acid [$C_6H_8O_7.H_2O$] and distilled water. TiO_2 sol was prepared by mixing titanium tetra-isopropoxide and distilled water at room temperature. Afterwards citric acid was added into the solution to adjucting pH. The solution was successively stirred till a clear and transparent acid sol was obtained. The TiO_2 sol was dried at 100 ºC in the oven. Then the gel was calcined at 550 ºC to prepare pure TiO_2 powders for about 80 min with a heating rate of about 10 ºC per minute in a muffle furnace. TiO_2 nanoparticles are abraviated as T0.

For the preparation of Zn-doped TiO_2 nanoparticles, the materials used were titanium tetra-isopropoxide [$Ti(OC_3H_7)_4$], zinc nitrate hexa hydrate [$Zn(NO_3)_26H_2O$], citric acid [$C_6H_8O_7.H_2O$]. TiO_2 sol was prepared by mixing titanium tetra-isopropoxide and distilled water at room temperature. After stirred the solution for 30 min, zinc nitrate hexa hydrate solution into the TiO_2 sol. Then 0.05 M citric acid were added into the solution to adjust the pH of the solution. Obtained sol was dried at 100 ºC in the oven for 43 h to get TiO_2 and thengel was calcined at 550 ºC to for about 80 min with a heating rate of about 10 ºC per minute in a furnace. Hereafter, the nanoparticles are named as as given in the Table 5.1.

Table 5. 1 Abbreviation of Zn doped TiO_2 nanoparticles

Sample	Abbreviation
Pure TiO_2	T0
Zn doped TiO_2	T1

5.2 Production of Electrodeposited Pure Nickel and Nickel Matrix Nanocomposite Coatings

Stainless steel with was selected as the substrate. The substrates previously polished using SiC paper from a grit of 400 to 1200 and chemically cleaned 20 seconds in etching solution which is given in Table 5.2. Finally, they were washed with distilled water.

Table 5. 2 Etching solution

Chemicals	Amount (vol%)
Nitric acid (HNO3)	2.5
Hydrochloric (HCl)	1.5
Hydrofluoric acid (HF)	1
Deionized water	95

Nickel coating and Ni matrix nanocomposite coatings were fabricated on substrate by electrodeposition at room temperature. A stainless steel and pure nickel plate were used as cathode and anode, respectively. Pure nickel coatings deposited from the Watts bath ($NiSO_4 \cdot 6H_2O$ 240-300 g/L, $NiCl_2 \cdot 6H_2O$ 40 g/L and H_3BO_3 30 g/L). Nickel sulfat concentration changed as 240, 280 and 300 g/L to investigate the effect of nickel sulfat concentration. The electrolytes were prepared by adding a range of 3 and 5 g/L of TiO_2 and Zn doped TiO_2 nanoparticles in Watts bath. All the coatings were electrodeposited with the direct current and deposition time of 15 min. The electrolyte composition and operating conditions are listed in Table 5.3 and 5.4, respectively. The electrolyte was composed of analytical reagents and distilled water. Prior to each experiment, the pH value of the as-performed electrolyte was adjusted into~ 4.5. To ensure uniform distribution of chemical compositions, the electrolyte was subject to the magnetic

stirring for 24 h at a rational rate of 471 rpm, also continued to mix ultrasonically during coating. After electrodeposition, the prepared coatings were cleaned with deionized water.

CHROMA 62050P-100-100 power supply was employed in all electrochemical deposition process. The coatings were named according to applied different current density and amount of particle concentration in Table 5.5.

Table 5. 3 Composition of the electrodeposition bath

Chemicals	**Amount of constituents (g/L)**
Nickel (II) Sulfate Hexahydrate $NiSO_4 \cdot 6H_2O$	240, 280 and 300
Nickel (III) Chloride Hexahydrate $NiCl_2 \cdot 6H_2O$	40
Boric Acid H_3BO_3	30
Sodium dodecyl sulfate (SDS)	1.5
Nanoparticle (TiO_2/Zn doped TiO_2)	3 and 5

Table 5. 4 Operating conditions of Nickel and Ni matrix nanocomposite coatings

Electrodeposition Parameters	
Particle size of TiO_2 and Zn doped TiO_2 nanoparticles (nm)	~70 and ~60
Concentration of TiO_2 and Zn doped TiO_2 nanoparticles (g/l)	3 and 5
Substrate	SS
Time (min)	15
Current Density (A.dm-2)	3, 5, 7
Temperature (°C)	45±1

Table 5.5 Abbreviation of the deposited coatings

Abbreviation	Nanoparticle	Concentration of Nanoparticle	Current Density (A dm^{-2})
NT 3-3	TiO_2	3	3
NT 3-5			5
NT 3-7			7
NT 5-3	TiO_2	5	3
NT 5-5			5
NT 5-7			7
NZT3-3	Zn doped TiO_2	3	3
NZT 3-5			5
NZT 3-7			7
NZT 5-3	Zn doped TiO_2	5	3
NZT 5-5			5
NZT 5-7			7

5.3 Characterization of the Nanoparticles and Nanocomposite Coatings

5.3.1 X-ray Diffraction (XRD)

X-ray diffraction has been commonly used for crystalline phases identification. The XRD measurement was performed by X-Ray Diffractometer (XRD, Rigaku, D/Max-2200/PC) with a grazing incident angle of 1° at 40 kV and 36 mA using Cu Kα radiation with a scanning speed of 4° 2θ/min.

The powder is irradiated with an X-ray of a known wavelength, λ, and hence diffraction of the X-ray takes place. The angle at which constructive interference occurs is then measured and the d spacings (the interplanar distances) of the crystals can be evaluated using Bragg's Law:

$$n\lambda = 2d\ sin\theta \tag{5.1}$$

where:

n = the order of diffraction (integer)

λ= incident X-ray wavelength (Å)

d = spacing between atomic layers in crystals (Å)

θ = angle between the incidence ray and the scattering plane (degrees)

The mean crystallite sizes may be obtained by the Scherrer equation:

$$D = \frac{k_{Sch}\lambda}{\beta_d cos\theta} \tag{5.2}$$

where:

D = crystalline size (Å)

k_{Sch} = Scherrer constant and equals to 0.93

λ= X-ray wavelength (1.542 Å)

βd = angular width of half-maximum intensity (degree)

θ= Bragg's angle (degree)

5.3.2 Particle Size Analyser

The laser diffraction particle size analyzer includes a laser device for generating an ultraviolet laser beam as a light source for generating a laser beam, and a fluorescent member closely attached to or disposed adjacent to a detecting surface of a photodiode array that measures the spatial intensity distribution of the diffracted and scattered light upon incidence thereof. A particle size distribution of the particles is calculated from a result of the measurementIn this study, Malvern Zeta Sizer Nano ZS90 device is used to determine size produced nanoparticles.

5.3.3 Scanning Electron Microscopy and Energy Dispersive Spectrum Analyse

A scanning electron microscope (SEM) scans a focused electron beam over a surface to create an image. The electrons in the beam interact with the sample, producing various signals that can be used to obtain information about the surface topography and composition.

The EDS detector separates the characteristic X-rays of different elements into an energy spectrum and EDS system software is used to analyze the energy spectrum in order to determine the abundance of specific elements. A typical EDS spectrum is portrayed as a plot of X-ray counts vs. energy (in keV). Energy peaks correspond to the various elements in the sample. Energy Dispersive X-ray Spectroscopy can be used to find the chemical composition of materials down to a spot size of a few microns and to create element composition maps over a much broader raster area. Together, these capabilities provide fundamental compositional information for a wide variety of materials, including polymers and metals.

In this study, the surface morphology and elemental composition of the coatings was examined by using JEOL-JSM 6060 Scanning Electron Microscopy with an Energy Dispersive X-ray spectroscopy (IXRF System EDS) system attachment.

5.3.4 Hardness

Hardness measurements involve making an indentation on the surface (or cross section for thin coatings) of the deposit. The indenter has a specified geometry and is applied with a specified load.

Microhardness tests were conducted on coated samples by applying 50 g of load for a period of 10 s using Vickers microhardness tester Shimadzu HMV Micro Hardness Tester. The test was carried out at five different locations of coatings surface and the average of all measurements was taken.

5.3.5 Electrochemical Mesurements

The electrochemical corrosion measurements were made using potentiostat/galvanostat/ZRA Gamry reference 600 with three electrodes cell with, Ni matrix nanocomposite coatings as the working electrode, graphite electrode as auxiliary electrode and Ag/AgCl electrode as reference electrode, respectively. The test solution for the corrosion investigations was a 3.5 (% wt) NaCl electrolyte at

temperature (25 ± 1ºC). Potentiodynamic polarization curves were recorded after 60 min open circuit potential(OCP) measurement from immersion of the Ni substrates in the test solution for corrosion. The open circuit potential of each specimen was monitored until a constant value was observed. Tafel measurements were carried out between -0.050 V and +0.050 V at 0.1667 mV/s scanning rate. The corrosion current density (icorr) for the specimens were determined by extrapolating the anodic and cathodic Tafel slopes. The potential range of measurements was investigated from0.30 V to 0.80 V vs Eoc, at a scan rate of 1 mV/s.

CHAPTER SIX
RESULTS AND DISCUSSION

6.1 Characterization of Sol-Gel Synthesized Nanoparticles

In this study, titanium dioxide and Zn doped TiO_2 nanoparticles were prepared using a sol-gel method. Characterization of obtained nanoparticles were performed by using XRD and particle size analysis.

The formation mechanism of sol-gel synthesized TiO_2 nanoparticles in this experiment could be explained as follows: during the synthesis process.

$$Ti(OR)4 + 4H_2O \xrightarrow{\text{hydrolysis}} 2Ti(OH)4 + 4ROH \quad (6.1)$$

$$Ti(OH)4 \xrightarrow{\text{condensation}} TiO2xH_2O + (2- x)\, H_2O \quad (6.2)$$

The X-ray patterns of the pure TiO_2 is shown in Figure 6.1. Anatase crystalline phase detected TiO_2 nanoparticles. The peaks at 2θ = 25.2◦, 37.8◦, 48.05◦, 53.8◦, 55.06◦,62.9◦, 68.7◦, 70.3◦, 75.03◦and 82.6◦are indexed to (101), (004), (200), (105), (211), (204), (116), (107) and (303) crystal planes of anatase with the JCPDS card no 21-1272.

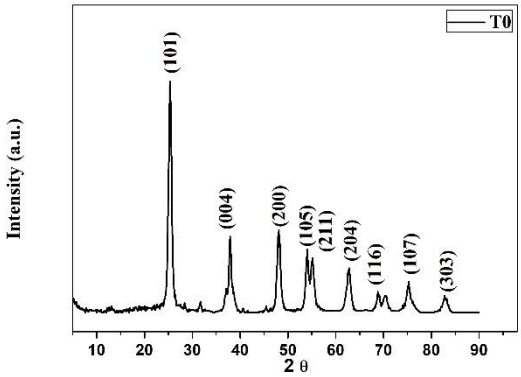

Figure 6.1 XRD patern of pure TiO_2 nanoparticle

Zn incorporation with different amounts ($Ti_{1-x}Zn_xO_2$, where x = 0.00, 0.025, 0.05, 0.075) was investigated in order to determine the effect of Zn on dimension of the produced nanoparticles. Abrreviation of the nanoparticles with different Zn incorporation are listed in Table 6.1. Zn incorpartion does not caused any different phase formation as given in Figure 6.2. All nanoparticles composed of anatase peaks at 2θ = 25.2◦, 37.8◦, 48.05◦, 53.8◦, 55.06◦,62.9◦, 68.7◦, 70.3◦, 75.03◦and 82.6 correspond to the reflections from (101), (004), (200), (105), (211), (204), (116), (107) and (303) crystal planes of the tetragonal titanium dioxide structure. All the diffraction peaks agreed with the reported JCPDS card No. 21-1272 for anatase. Crystallinity and particle size values of TiO_2 and Zn doped TiO_2 nanoparticles was given in Table 6.1.

The particle size was also calculated and verified using Scherrer formula. The crystallinity and particle size values of nanoparticles are given in Table 6.1.

$$D = 0.9\lambda \,/\, \beta \cos\theta \tag{6.3}$$

Where is λ the wavelength of X-ray radiation, β is the full width at half maximum (FWHM) of the peaks.

Table 6.1 Crystallinity and particle size values of TiO_2 and Zn doped TiO_2 nanoparticles

Sample	Particle size (nm)	Crystallinity (nm)
T0	68.70	33.8
T1-1 (0.025 Zn)	77.26	19.3
T1-2 (0.050 Zn)	57.67	20.1
T1-3 (0.075 Zn)	63.46	21.5

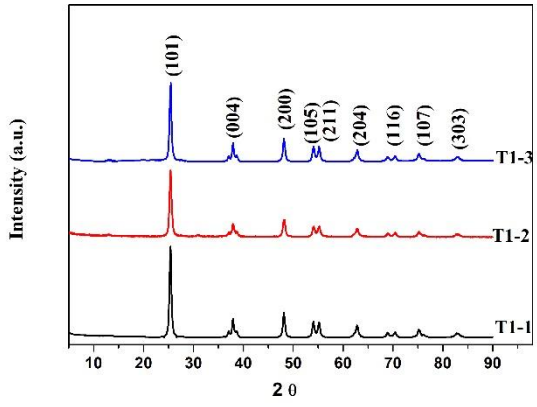

Figure 6.2 XRD pattern of Zn doped TiO_2 nanoparticles

Particle sizes of nanoparticles were measured using Malvern Zeta Sizer Nano ZS90. Results of the particle size analysis of TiO_2 and Zn doped TiO_2 nanoparticles are given in Figure 6.3. Dimension of the nanoparticles are close to each other with value of ~70 nm and 60 nm for TiO_2 and Zn doped TiO_2 nanoparticles, respectively. Ni-Zn/TiO_2 nanocomposites were deposited with Zn doped TiO_2 nanoparticles with 0.005 Zn concentration.

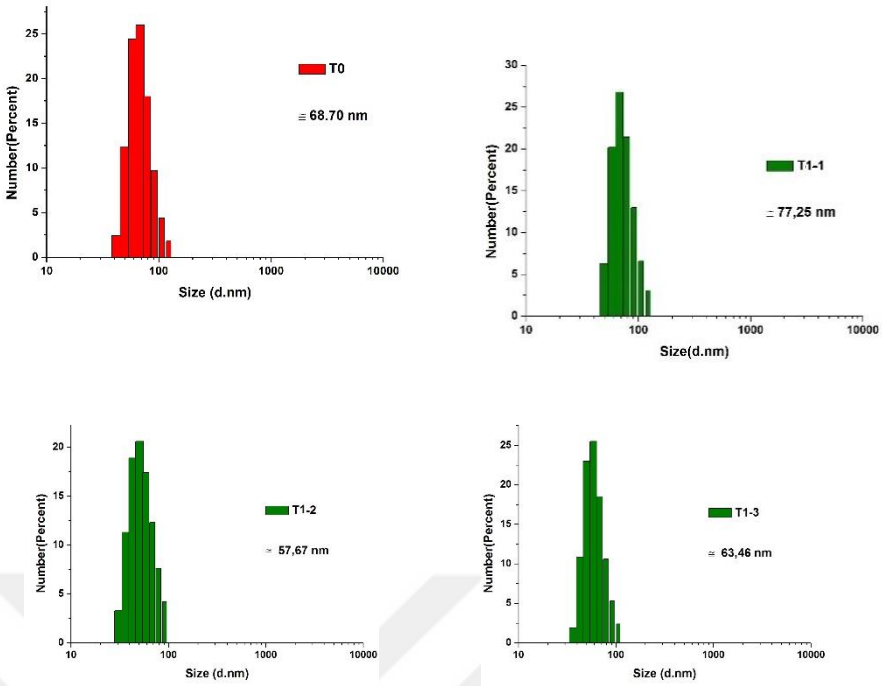

Figure 6.3 Distribution chart of particle sizes of TiO_2 and Zn doped TiO_2 nanoparticles

6.2 Characterization of Electrodeposited Nickel and Nickel Matrix Nanocomposite Coatings

6.2.1 Characterization of Electrodeposited Ni Coatings

Pure nickel coatings on steel substrates were electrodeposited from nickel Watts bath with varying nickel sulfate concentrations of 240, 280 and 300 g/L. Deposition bath composition and abbreviation of the samples are given in Table 6.2.

Table 6.2 Composition of the electrodeposition bath and abbreviation of deposited pure nickel coatings

Chemicals	**Deposition bath composition (g/L)**		
Nickel (II) sulfate hexahydrate	N1	N2	N3
($NiSO_4.6H_2O$)	240	280	300
Nickel (III) chloride hexahydrate ($NiCl_2.6H_2O$)	40		
Boric acid (H_3BO_3)	30		

Detailed investigations on the effect of deposition bath composition in terms of amount of nickel (II) sulfate hexahydrate constituent on the evolution of surface morphology, microhardness, and corrosion of pure nickel coatings are presented. Figure 6.4 present X-ray diffraction patterns of pure nickel coatings deposited at constant current density 3 mA dm^{-2}. Results showed that typical characteristic peaks of nickel at 44.48°, 51.83° and 76.35° corresponding to (111), (200) and (220) crystallographic planes of nickel respectively (Nickel XRD JCPDS Ref. No. 70-1849) (Rostami, Moghaddam, & Asgari, 2013). According to the pattern, (111) and (200) planes are the main diffractions. Crystals of all coatings tend to grow in two directions of (111) and (200) planes. It can be seen that increament of nickel sulfate content in the electrolyte results in increament of the intensity of (200) peaks and it becomes the main diffraction plane.

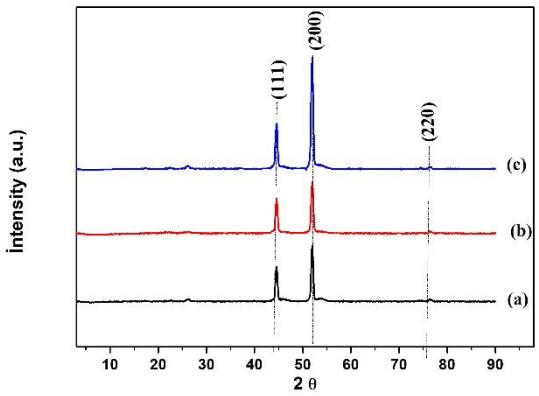

Figure 6.4 XRD pattern of deposited pure nickel coatings (a) N1, (b) N2 and (c) N3

Figure 6.5 (a, b and c) shows the SEM morphologies of deposited coatings. SEM micrograph of the Ni coating represented in Figure 6.5 exhibit a homogeneous structure with regular pyramidal shape. typical for nickel crystallites (Mohajeri, Dolati, & Rezagholibeiki, 2011).

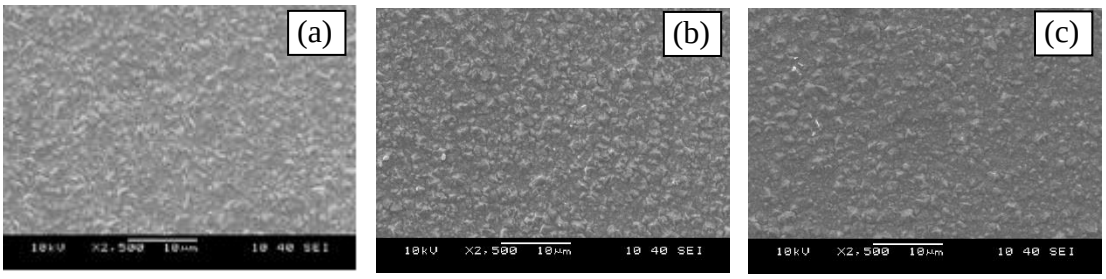

Figure 6.5 SEM images of deposited pure nickel coatings (a) N1, (b) N2 and (c) N3

Microhardness, a measure of resistance to deformation under indentation was estimated using a Vickers microhardness tester. The microhardness of deposited pure Ni coatings electrodeposited at different nickel sülfate concentration. Figure 6.6 shows the hardness graph of pure nickel coatings. The hardness values of coatings were measured as 198.8 HV, 289.2 HV and 357 HV for coatings N1, N2 and N3, respectively. Results indicate that hardness value of the coatings decreased with incresing nickel sulfate concentartion in the Watts bath.

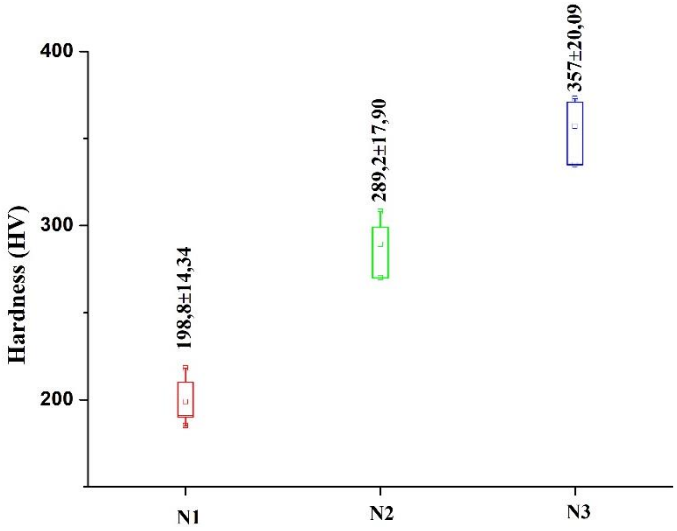

Figure 6.6 The hardness values of deposited pure Ni coatings

Figure 6.7 show the potantiodynamic measurementsof pure nickel coatings in 3.5% NaCl solution.

Table 6.3 lists the corrosion properties of the püre nickel coatings. According to these data, the corrosion current density (icorr) of the coatings is increased 4.928 $\mu A/cm^2$ to 6.390 $\mu A/cm^2$ with increment of pure nickel sulfate concentration in the

electrolyte. Corrosion properties of the nickel coating named as N1 better than other coatings. Watts bath with minumum nickel sulfate (240 g/L) concentration was selected as deposition electrolyte to produce nanocomposite coatings because of the superior corrosion properties.

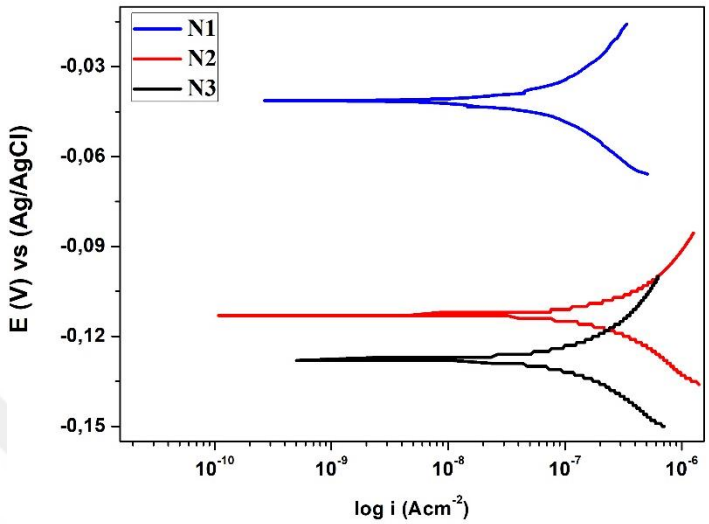

Figure 6.7 Potentiodynamic curves of deposited pure Ni coatings

Table 6.3 Corrosion data of the pure nickel coatings

Coating name	Corrosion potential (V)	Corrosion current density (µA/cm^2)	Corrosion rate (MPY)
N1	-0.041	4.928	0.693
N2	-0.110	6.390	1.153
N3	.-0.127	5.052	0.798

6.2.2 Characterization of Electrodeposited Ni-TiO_2 and Ni-Zn/TiO_2 Nanocomposite Coatings

The influence of TiO_2 and Zn doped TiO_2 nanoparticles incorporation into the Ni matrix on crystal structure of the deposited nanocoposite was investigated by XRD. Figure 6.8 shows the XRD patterns of pure nickel coating and Ni-TiO_2 nanocomposite coatings deposited at different TiO_2 concentration (3 g/L and 5 g/L) under the current conditions of 3 A.dm^{-2}, 5 A dm^{-2} and 7 A dm^{-2}. X-ray diffraction patterns of deposited coatings are characterized by (111), (200), and (220) diffraction peaks of Ni phase (JCPDS 70-1849). That implies nickel coatings are successfully deposited on the steel

substrates. The growth of Ni coatings with TiO_2 addition was dominated by the (200) crystal surface and the (200) peak intensity was increased. The change in the deposition current density conditions and nanoparticle concentration altered neither the preferred orientation of a plane nor the phase structure of the coatings obtained. On the other hand, (200) peak intensity increases with increasing TiO_2 nanocomposite content in the elecyrolyte and applied current density conditions. Figure 6.9 shows the XRD pattern of the Ni-Zn/TiO_2 nanocomposite coatings deposited at different TiO_2 concentration (3 g/L and 5 g/L) under the current conditions of 3 A.dm^{-2}, 5 A dm^{-2}. Ni-Zn/TiO_2 nanocomposite coatings XRD pattern similar to that of Ni-TiO_2 nanocomposite coatings in terms of phase structure and preferred orientation of a plane. Crystallinity values of TiO_2 and Zn doped TiO_2 nanoparticles are given in Table 6.4.

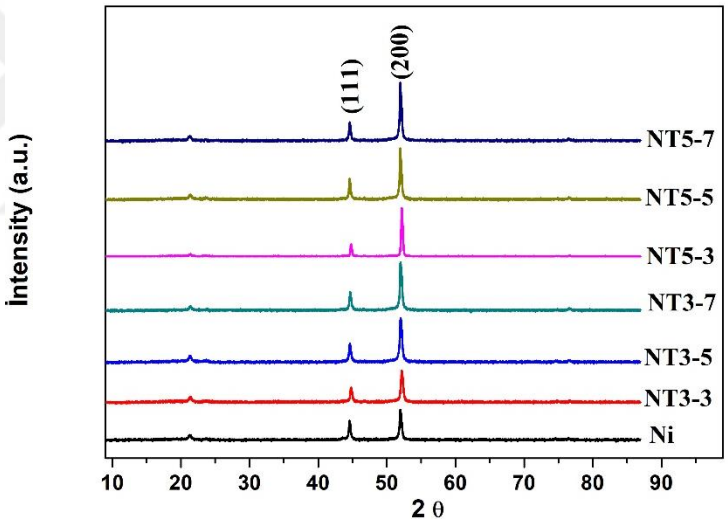

Figure 6.8 XRD patterns of the nickel coatings and Ni-TiO_2 nanocomposite coatings

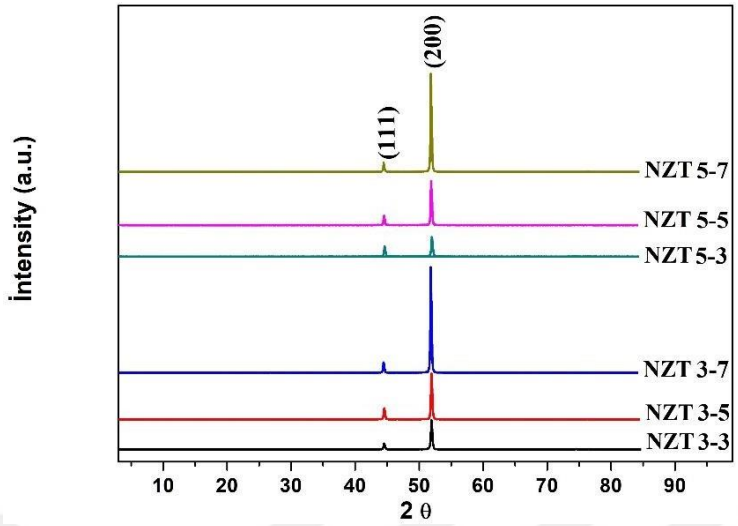

Figure 6.9 XRD patterns of the Ni-Zn/TiO_2 nanocomposite coatings

Table 6.4 Crystallinity values of produced coatings

Sample	Crystallinity (nm)
N1	29.81
N2	31.86
N3	24.98
NT3-3	28.01
NT3-5	24.31
NT3-7	26.39
NT5-3	35.51
NT5-5	30.78
NT5-7	28.86
NZT3-3	31.84
NZT3-5	35.51
NZT3-7	38.45
NZT5-3	34.2
NZT5-5	38.46
NZT5-7	38.45

SEM images of Ni-TiO_2 nanocomposite coatings deposited at different TiO_2 concentration and current densities are indicated in Figure 6.10. It is observed that the coatings are homogeneous without cracks and with dense morphology that covers entire substrate surface area.

SEM images of Ni/TiO_2 nanocomposite coatings also reveal a reduction of Ni crystallites grain size due to the presence of TiO_2 nanoparticles reinforced compared with those of pure Ni coating prepared under similar conditions. The same tendency of crystallite sizes reduction was observed also by Gyftou et al. (Gyftou, Pavlatou, & Spyrellis, 2008) for Ni/SiC coatings when it was compared with pure Ni coating. This crystallite sizes reduction can be explained by the incorporation of TiO_2 nanoparticles at the borders and the edges of the nickel crystallites due to their very small size. Additionally, crystallite grain size was increased with increasing current density.

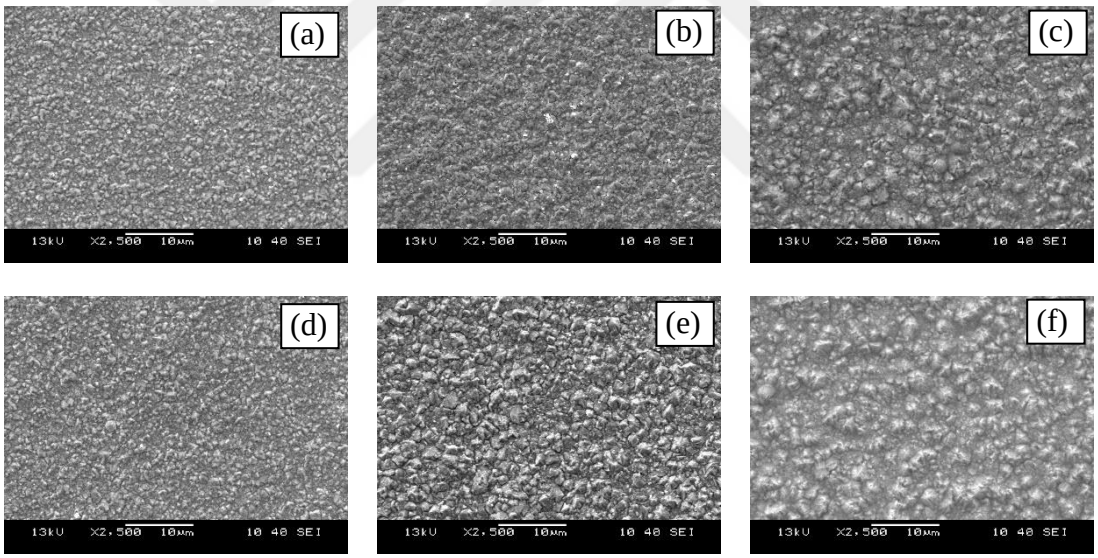

Figure 6.10 SEM images of Ni-TiO_2 nanocomposite coatings deposited at different TiO_2 concentration and current densities: (a) 3 g/L, 3 A/dm^2, (b)3 g/L, 5 A/dm^2, (c) 3 g/L, 7 A/dm^2, (d)5 g/L, 3 A/dm^2, (e)5 g/L, 5 A/dm^2, (f) 5 g/L, 7 A/dm^2

SEM images of Ni-Zn/TiO_2 nanocomposite coatings deposited at different Zn doped TiO_2 concentration and current densities are indicated in Figure 6.11(a)–(f). It is observed that the coatings are uniform without cracks and homogeneous structure. As nanoparticle concentration increased (3 to 5 g/L), the grains become compact and homogenously arranged.

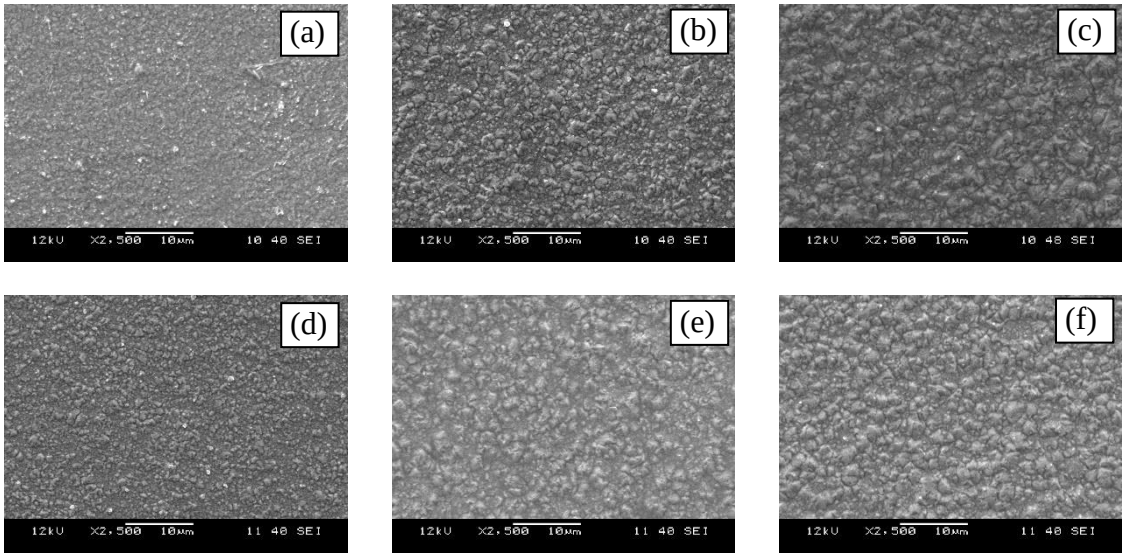

Figure 6.11 SEM images of Ni-Zn/TiO_2 nanocomposite coatings deposited at different TiO_2 concentration and current densities: (a) 3 g/L, 3 A/dm^2, (b)3 g/L, 5 A/dm^2, (c) 3 g/L, 7 A/dm^2, (d)5 g/L, 3 A/dm^2, (e)5 g/L, 5 A/dm^2, (f) 5 g/L, 7 A/dm^2

The coating thickness was measured by Electrophysik coating thickness gauge, and then calculated by averaging over five tests for each sample. The measurement results are given in Table 6.5. As can be seen, a coating with an average thickness of 48.72 ± 3.27 μm is uniformly deposited on the steel substrate, with no detectable porosity and cracks in the coating and coating/substrate interface (Figure 6.12 and 6.13) In addition, a homogeneous distribution of the nano particles throughout the Ni matrix is confirmed.

Since the nanoparticle reinforcement can modify the microstructure of the Ni coating and act as an inert physical barrier to diffuse the corrosive species in the coating thickness, the corrosion resistance of the coating can be improved considerably by the nanoparticle incorporation (Aruna, Grips, & Rajam, 2009).

Table 6.5 Thickness values of nanocomposite coatings

Coating name	Coating Thickness
NT3-3	45,08
NT 3-5	45,44
NT 3-7	50,38
NT 5-3	48,98
NT 5-5	46,98
NT 5-7	45,38
NZT3-3	48,72
NZT 3-5	49,60
NZT 3-7	52,18
NZT 5-3	55,68
NZT 5-5	50,90
NZT 5-7	45,42

The microhardness of pure Ni coating and nanocomposite coatings are indicated in Figure 6.12. It was found that the hardness values of Ni–TiO_2 and Ni-Zn /TiO_2 nanocomposite coatings are higher than that of pure Ni coatings (198 HV). Besides, obtained results showed that increasing nanoparticle concentration increases the hardness of Ni-TiO_2 and Ni-Zn/TiO_2 nanocomposite coatings.

Hardness values of the Ni-TiO_2 and Ni-Zn/TiO_2 nanocomposite coatings in the range of 303-477 HV. The increase in hardness of nanocomposite coatings can be due to two reasons: 1) The grain refinement based on Hall-Patch effect can lead to increased hardness of the coatings (Srivastava, Grips, & Rajam, 2007; N. Wang, Wang, Aust, & Erb, 1995).2) By increasing the nanoparticles in the coatings, their hardness is increased by the dispersion hardening based on Orowan's mechanism (Dieter & Bacon, 1986). This strengthening mechanism is activated by increasing the amount of reinforcing nanoparticles in nanocomposite coatings (Baghery et al., 2010; Juneghani, Farzam, & Zohdirad, 2013).

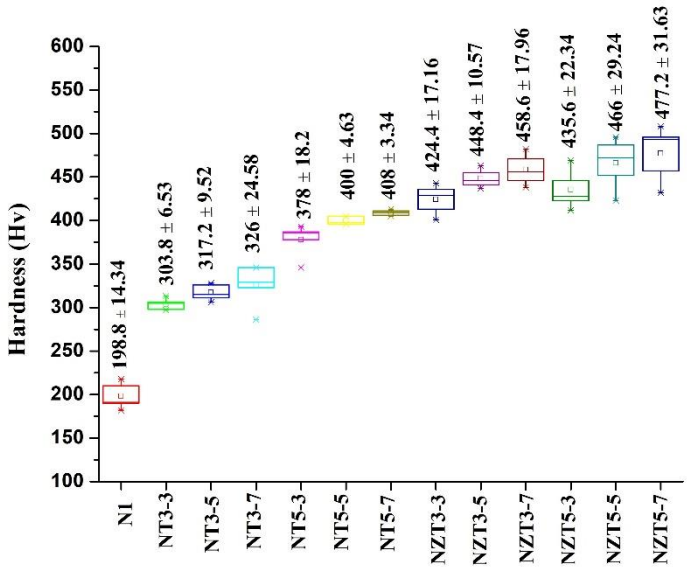

Figure 6.12 Microhardness values of coatings

6.3 Corrosion Behavior of Electrodeposited Nanocomposite Coatings

The open circuit potential (E_{OC}, vs. Ag/AgCl) was measured and used to ensure the stability of measured system. Figure 6.13 is the E_{OC} value vs. immersion time curves of nanocomposite coatings with 5g/L nanoparticle concenration at different current densitiesin NaCl solution at 25±1 ºC. Based on the observed results from the E_{OC} value for all the specimens, the tendency of E_{OC} curves shifted towards a stable direction and reached a steady state condition at a short period, as indicative of the stability of measured system. Negative potential connected with an unstable state is indicative of the active dissolution and responsible localized corrosion at the exposed coating surface. This result was associated with the coating's structure and surface properties, indicating that a decreasing of defective boundaries or micro pores existing on the coating's surface reduced the short-circuit diffusion paths for diffusion behavior by aggressive ions (Cl^-, etc.) where occurred at the corroded surfaces (Meng et al., 2010).

Nickel composite coatings have better corrosion resistance than pure nickel coatings because reinforced second phase particles disturb the regular growth of nickel crystal and promote new nucleation site. This makes structure of composite coatings more finely crystalline and hence improved corrosion resistance of composite coatings

(Amadeh et al., 2010; Szczygieł & Kołodziej, 2005). Addition of these particles in composite coatings will decrease corrosion current density and will shift corrosion potential of composite coatings towards more noble direction i.e. positive value. Amadeh *et al.* performed electrochemical experiments to analyze corrosion behavior of (Ni-SiC) composite coatings(Amadeh et al., 2010). Addition of nano particles act as obstacles to the initiation and development of defect corrosion and also filled in crevice, gaps, and micron holes of nickel matrix resulting in significant improvement of corrosion resistance of composite coatings(Vaezi et al., 2008).

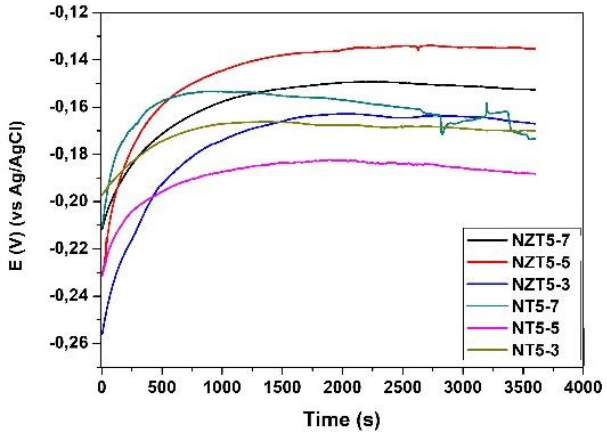

Figure 6.13 Open circuit potential as a function of time of nanocomposite coatings

Figure 6.14 shows potentiodynamic polarization behaviour of produced nanocomposite coatings. Results show that the corrosion resistance of nanocomposite coatings has significantly improved compared to nickel coatings.

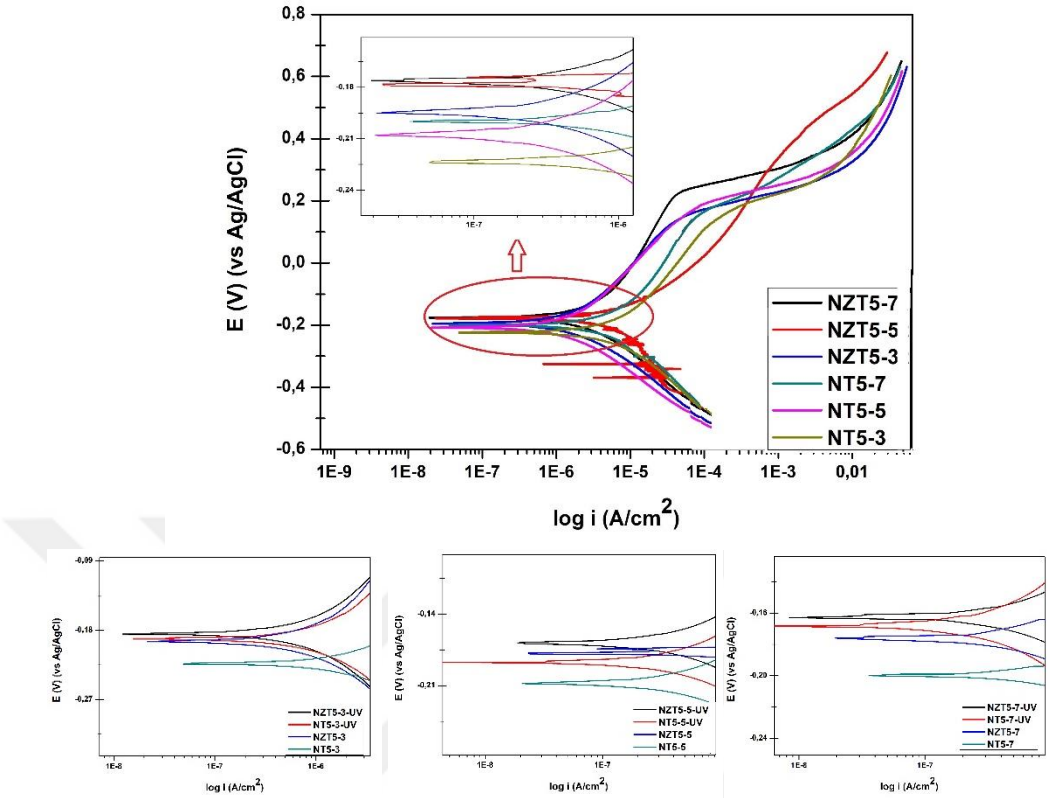

Figure 6.14 Potentiodynamic polarization curves of the nanocomposite coatings

From the viewpoint of corrosion protection, noble potentials or lower corrosion current densities are of significance so as to achieve an appropriate protection. NZT 5-7 nanocomposite coating have better corrosion performance compared to other nanocomposite coatings.

In the second step corrosion tests were carried out after nanocomposite coatings were exposured to UV light in order to investigate the effect of UV irradiation on corrosion resistance.

In the semiconductor, electrons in the valence band are excited to the conduction band under irradiation with appropriate light. The excited electrons are injected to the metal so as to keep its potential more negative than the corrosion potential. After the UV light is turned off, electrons that have been stored in the electron pool are injected to the metal so that it is still protected from corrosion (Tatsuma, Saitoh, Ohko, &

Fujishima, 2001). In a similar study, Tsujikawa et al. have prepared a multilayer-coated carbon steel, amorphous TiO_2/anatase TiO_2/Ti-Fe oxide/R-Fe_2O_3/Fe, and found that the coated steel retains its anticorrosion effect for a while even in the dark after UV irradiation (J. Huang, Shinohara, & Tsujikawa, 1999). Similar results were obtained with Tsujikawa et al., and corrosion protection was increased according to the corrosion test results made in the dark after the UV irradiation, additionly, corrosion rates are reduced (J. Huang et al., 1999) (Figure 6.15).

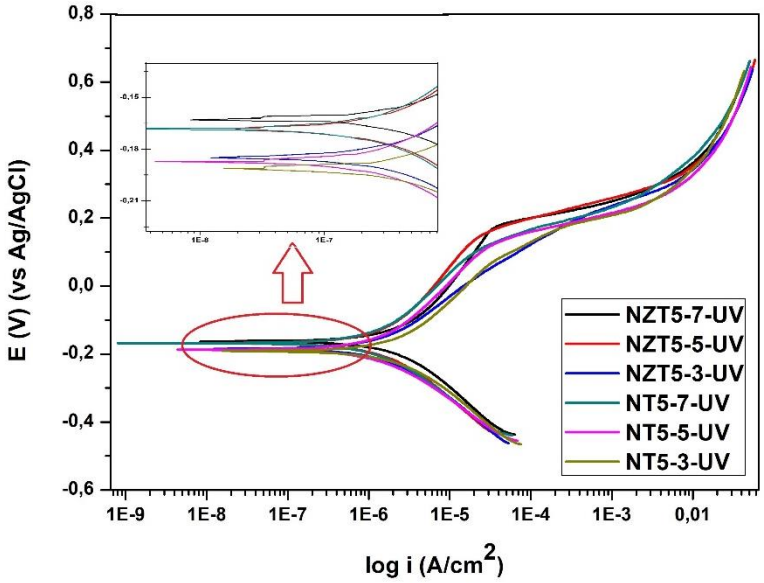

Figure 6.15 Potentiodynamic polarization curves of the nanocomposite coatings after UV illumination

CHAPTER SEVEN
CONCLUSION

In this thesis, TiO_2 and Zn doped TiO_2 nanoparticles were produced by sol-gel method. Then, Ni matrix nanocomposite coatings were prepared by electrodeposition technique on steel substrates. Different amount of TiO_2 and Zn doped TiO_2 nanoparticles was added in deposition electrolyte to investigate the effect of particle concentration on the structural and corrosion properties of obtained nanocomposite coatings.

Findings achieved from the experimental works can be summarized as follows:

TiO_2 and Zn doped TiO_2 nanoparticles were successfully produced by sol-gel method.

According to XRD results, TiO_2 and Zn doped TiO_2 nanoparticles are composed of pure anatase phases and average particle sizes were measured ~70 nm and ~60 nm, respectively.

Ni matrix nanocomposite coatings were produced by electrodeposition technique with addition of TiO_2 or Zn doped TiO_2 nanoparticles into the Watts bath.

The XRD results show typical characteristic peaks of nickel at 44.48°, 51.83° and 76.35° corresponding to (111), (200) and (220) crystallographic planes for deposited coatings

The presence of nanoparticles in the nanocomposite coatings were confirmed by EDS-mapping analysis.

Obtained coatings with TiO_2 nanoparticle addition have higher hardness value.

It can be concluded that addition of TiO_2 or Zn doped TiO_2 nanoparticles in the deposition electrolyte enhanced corrosion behavior of coatings .

REFERENCES

Adesina, A. (2004). Industrial exploitation of photocatalysis: progress, perspectives and prospects. *Catalysis Surveys from Asia, 8*(4), 265-273.

Ahmad, Y. H., & Mohamed, A. (2014). Electrodeposition of nanostructured nickel-ceramic composite coatings: A review.

Amadeh, A., Rahimi, A., Farshchian, B., & Moradi, H. (2010). Corrosion Behavior of Pulse Electrodeposited Nanostructure Ni–SiC Composite Coatings. *Journal of nanoscience and nanotechnology*, *10*(8), 5383-5388.

An, B.-G., Li, L.-X., & Li, H.-X. (2008). Electrodeposition in the Ni-plating bath containing multi-walled carbon nanotubes. *Materials Chemistry and Physics, 110*(2), 481-485.

Arai, S., Fujimori, A., Murai, M., & Endo, M. (2008). Excellent solid lubrication of electrodeposited nickel-multiwalled carbon nanotube composite films. *Materials letters, 62*(20), 3545-3548.

Aslani, A., & Oroojpour, V. (2011). CO gas sensing of CuO nanostructures, synthesized by an assisted solvothermal wet chemical route. *Physica B: Condensed Matter, 406*(2), 144-149.

Atchudan, R., Edison, T. N. J. I., Perumal, S., Karthikeyan, D., & Lee, Y. R. (2017). Effective photocatalytic degradation of anthropogenic dyes using graphene oxide grafting titanium dioxide nanoparticles under UV-light irradiation. *Journal of Photochemistry and Photobiology A: Chemistry, 333*, 92-104.

Baghery, P., Farzam, M., Mousavi, A., & Hosseini, M. (2010). Ni–TiO 2 nanocomposite coating with high resistance to corrosion and wear. *Surface and Coatings Technology*, *204*(23), 3804-3810.

Bailey, S., Baldini, N., Barkley, E., Peters, K., Rosiak, J., Simms, S., Wilhelm, R. (2003). Annual book of ASTM standards: metals—mechanical testing; elevated and low temperature tests; metallography. *West Conshohocken, PA: ASTM International*, 61-82.

Bapu, G. R., & Jayakrishnan, S. (2012). Development and characterization of electro deposited Nickel–Titanium Carbo Nitride (TiCN) metal matrix nanocomposite deposits. *Surface and Coatings Technology, 206*(8), 2330-2336.

Beckel, D., Bieberle-Hütter, A., Harvey, A., Infortuna, A., Muecke, U., Prestat, M., Gauckler, L. (2007). Thin films for micro solid oxide fuel cells. *Journal of Power Sources, 173*(1), 325-345.

Bełtowska-Lehman, E., Goral, A., & Indyka, P. (2011). Electrodeposition and characterization of Ni/Al2O3 nanocomposite coatings. *Archives of Metallurgy and Materials, 56*(4), 919-931.

Benjamin, J. S. (1970). Dispersion strengthened superalloys by mechanical alloying. *Metallurgical transactions, 1*(10), 2943-2951.

Bensebaa, F. (2012). *Nanoparticle Technologies: Chapter 2. Wet Production Methods* (Vol. 19): Elsevier Inc. Chapters.

Brinker, C., Keefer, K., Schaefer, D., & Ashley, C. (1982). Sol-gel transition in simple silicates. *Journal of Non-Crystalline Solids, 48*(1), 47-64.

Brinker, C., Keefer, K., Schaefer, D., Assink, R., Kay, B., & Ashley, C. (1984). Sol-gel transition in simple silicates II. *Journal of Non-Crystalline Solids, 63*(1), 45-59.

Brinker, C. J., & Scherer, G. W. (2013). *Sol-gel science: the physics and chemistry of sol-gel processing*: Academic press.

Camargo, P. H. C., Satyanarayana, K. G., & Wypych, F. (2009). Nanocomposites: synthesis, structure, properties and new application opportunities. *Materials Research, 12*(1), 1-39.

Chen, L., Wang, L., Zeng, Z., & Xu, T. (2006). Influence of pulse frequency on the microstructure and wear resistance of electrodeposited Ni–Al 2 O 3 composite coatings. *Surface and Coatings Technology, 201*(3), 599-605.

Chen, Y., Lunsford, S., & Dionysiou, D. D. (2009). Characterization and electrochemical response of sonogel carbon electrode modified with nanostructured zirconium dioxide film. *Sensors and Actuators B: Chemical, 137*(1), 291-296.

Daraio, C., & Jin, S. (2012). Synthesis and patterning methods for nanostructures useful for biological applications *Nanotechnology for Biology and Medicine* (pp. 27-44): Springer.

Davis, J. R. (2000). *Nickel, cobalt, and their alloys*: ASM international.

De Jonghe, L. C., & Rahaman, M. N. (2003). 4.1 Sintering of Ceramics. *Handbook of Advanced Ceramics: Materials, Applications, Processing and Properties, 2*, 187.

Dhand, C., Dwivedi, N., Loh, X. J., Ying, A. N. J., Verma, N. K., Beuerman, R. W.,. Ramakrishna, S. (2015). Methods and strategies for the synthesis of diverse nanoparticles and their applications: a comprehensive overview. *Rsc Advances, 5*(127), 105003-105037.

Dieter, G. E., & Bacon, D. J. (1986). *Mechanical metallurgy* (Vol. 3): McGraw-Hill New York.

Dubey, R., Rajesh, Y., & More, M. (2015). Synthesis and Characterization of SiO2 Nanoparticles via Sol-gel Method for Industrial Applications. *Materials Today: Proceedings, 2*(4-5), 3575-3579.

Fricke, J., & Reichenauer, G. (1987). Structural investigaticn CF SiO2—aerogels. *Journal of Non-Crystalline Solids, 95*, 1135-1141.

Gan, J. A., & Berndt, C. C. (2015). Nanocomposite coatings: thermal spray processing, microstructure and performance. *International materials reviews, 60*(4), 195-244.

Gan, Y. X. (2012). Structural assessment of nanocomposites. *Micron, 43*(7), 782-817.

Ghaziof, S., & Gao, W. (2015). Zn–Ni–Al 2 O 3 nano-composite coatings prepared by sol-enhanced electroplating. *Applied Surface Science, 351*, 869-879.

Giesche, H. (1994). Synthesis of monodispersed silica powders II. Controlled growth reaction and continuous production process. *Journal of the European Ceramic Society, 14*(3), 205-214.

Guglielmi, N. (1972). Kinetics of the deposition of inert particles from electrolytic baths. *Journal of the Electrochemical Society, 119*(8), 1009-1012.

Gyftou, P., Pavlatou, E., & Spyrellis, N. (2008). Effect of pulse electrodeposition parameters on the properties of Ni/nano-SiC composites. *Applied Surface Science, 254*(18), 5910-5916.

Hellstern, E., Fecht, H. J., Fu, Z., & Johnson, W. (1989). Structural and thermodynamic properties of heavily mechanically deformed Ru and AlRu. *Journal of applied physics, 65*(1), 305-310.

Hitchman, M. L., & Jensen, K. F. (1993). *Chemical vapor deposition: principles and applications* (Vol. 21): Academic Press London.

Hosseini, S., Gholami, A., Koranian, P., Nemati, M., Madaeni, S., & Moghadassi, A. (2014). Electrochemical characterization of mixed matrix heterogeneous cation exchange membrane modified by aluminum oxide nanoparticles: mono/bivalent ionic transportation. *Journal of the Taiwan Institute of Chemical Engineers, 45*(4), 1241-1248.

Hou, K., Ger, M., Wang, L., & Ke, S. (2002). The wear behaviour of electro-codeposited Ni–SiC composites. *Wear, 253*(9), 994-1003.

Hovestad, A., & Janssen, L. (1995). Electrochemical codeposition of inert particles in a metallic matrix. *Journal of Applied Electrochemistry, 25*(6), 519-527.

Huang, B.-L., Perez, R., Lavernia, E., & Luton, M. (1996). Formation of supersaturated solid solutions by mechanical alloying. *Nanostructured Materials, 7*(1), 67-79.

Huang, J., Shinohara, T., & Tsujikawa, S. (1999). Protection of carbon steel from atmospheric corrosion by TiO2 coating. *Zairyo-to-Kankyo, 48*(9), 575-582.

Iler, R. (1979). The chemistry of silica.,(Wiley-Interscience: New York).

Ishio, S., Narisawa, T., Takahashi, S., Kamata, Y., Shibata, S., Hasegawa, T., Kondo, Y. (2012). L1 0 FePt thin films with [001] crystalline growth fabricated by SiO 2 addition—rapid thermal annealing and dot patterning of the films. *Journal of Magnetism and Magnetic Materials, 324*(3), 295-302.

Juneghani, M. A., Farzam, M., & Zohdirad, H. (2013). Wear and corrosion resistance and electroplating characteristics of electrodeposited Cr–SiC nano-composite coatings. *Transactions of Nonferrous Metals Society of China*, *23*(7), 1993-2001.

Kim, S.-I., Lee, J.-S., Ahn, H.-J., Song, H.-K., & Jang, J.-H. (2013). Facile route to an efficient NiO supercapacitor with a three-dimensional nanonetwork morphology. *ACS applied materials & interfaces*, *5*(5), 1596-1603.

Kim, S. K., & Yoo, H. J. (1998). Formation of bilayer Ni–SiC composite coatings by electrodeposition. *Surface and coatings Technology, 108*, 564-569.

Koch, C. (1993). The synthesis and structure of nanocrystalline materials produced by mechanical attrition: A review. *Nanostructured Materials, 2*(2), 109-129.

Kumar, A., Yadav, N., Bhatt, M., Mishra, N. K., Chaudhary, P., & Singh, R. (2015). Sol-Gel Derived Nanomaterials and It's Applications: A Review. *Research Journal of Chemical Sciences ISSN, 2231*, 606X.

Kumar, S. A., & Denchev, Z. (2009). Development and characterization of phosphorus-containing siliconized epoxy resin coatings. *Progress in Organic Coatings, 66*(1), 1-7.

Kumar, V., Masudy-Panah, S., Tan, C., Wong, T., Chi, D., & Dalapati, G. (2013). *Copper oxide based low cost thin film solar cells.* Paper presented at the Nanoelectronics Conference (INEC), 2013 IEEE 5th International.

Kuo, S.-L., Chen, Y.-C., Ger, M.-D., & Hwu, W.-H. (2004). Nano-particles dispersion effect on Ni/Al 2 O 3 composite coatings. *Materials Chemistry and Physics, 86*(1), 5-10.

Leary, R., & Westwood, A. (2011). Carbonaceous nanomaterials for the enhancement of TiO 2 photocatalysis. *Carbon, 49*(3), 741-772.

Liu, X., Jiang, Z., Li, J., Zhang, Z., & Ren, L. (2010). Super-hydrophobic property of nano-sized cupric oxide films. *Surface and Coatings Technology, 204*(20), 3200-3204.

Lukaszkowicz, K. (2011). Review of nanocomposite thin films and coatings deposited by PVD and CVD technology *Nanomaterials*: InTech.

Martínez-Martínez, D. (2013). Nanocomposite Coatings *Encyclopedia of Tribology* (pp. 2359-2364): Springer.

Meng, G., Sun, F., Shaoa, Y., Zhang, T., Wang, F., Dong, C., & Li, X. (2010). Effect of phytic acid on the microstructure and corrosion resistance of Ni coating. *Electrochimica Acta, 55*(20), 5990-5995.

Mohajeri, S., Dolati, A., & Rezagholibeiki, S. (2011). Electrodeposition of Ni/WC nano composite in sulfate solution. *Materials Chemistry and Physics, 129*(3), 746-750.

Mohammadi, M., & Fray, D. (2010). Low temperature nanostructured zinc titanate by an aqueous particulate sol–gel route: Optimisation of heat treatment condition based on Zn: Ti molar ratio. *Journal of the European Ceramic Society, 30*(4), 947-961.

Nagajyothi, P., Muthuraman, P., Sreekanth, T., Kim, D. H., & Shim, J. (2017). Green synthesis: in-vitro anticancer activity of copper oxide nanoparticles against human cervical carcinoma cells. *Arabian Journal of Chemistry, 10*(2), 215-225.

Nasirpouri, F. (2017). Electrodeposited Nanocomposite Films *Electrodeposition of Nanostructured Materials* (pp. 289-310): Springer.

Natter, H., & Hempelmann, R. (2008). Nanocrystalline metals prepared by electrodeposition. *Zeitschrift für Physikalische Chemie, 222*(2-3/2008), 319-354.

Nava, O., Luque, P., Gómez-Gutiérrez, C., Vilchis-Nestor, A., Castro-Beltrán, A., Mota-González, M., & Olivas, A. (2017). Influence of Camellia sinensis extract on Zinc Oxide nanoparticle green synthesis. *Journal of Molecular Structure, 1134*, 121-125.

Niaki, A. G., Bakhshayesh, A., & Mohammadi, M. (2014). Double-layer dye-sensitized solar cells based on Zn-doped TiO 2 transparent and light scattering layers: improving electron injection and light scattering effect. *Solar Energy, 103*, 210-222.

Niederberger, M., & Pinna, N. (2009). *Metal oxide nanoparticles in organic solvents: synthesis, formation, assembly and application*: Springer Science & Business Media.

Nurlaela, E., Chong, F. K., Dutta, B. K., & Riaz, N. (2010). *Bimetallic Cu-Ni/TiO2 as photocatalyst for hydrogen production from water*. Paper presented at the International Conference on Fundamental and Applied Sciences (ICFAS2010).

Pereira, R. F. d. C., Oliveira, E. S. D. d., Vieira, M. R. S., Lima, M. A. G. d. A., & Urtiga Filho, S. L. (2017). Evaluation of Co-Ni/SiC Nanocomposite Coating Obtained by Electrodeposition on the Corrosion Resistance of API 5L X80 Steel. *Materials Research*(AHEAD), 0-0.

Pierre, A. (1998). Introduction to Sol–Gel ProcessingKluwer International Series in Sol–Gel Processing: Technology and Applications: Kluwer, Dordrecht.

Pompei, E., Magagnin, L., Lecis, N., & Cavallotti, P. (2009). Electrodeposition of nickel–BN composite coatings. *Electrochimica Acta, 54*(9), 2571-2574.

Qiao, L.-y., Xie, F.-y., Xie, M.-h., Gong, C.-h., Wang, W.-l., & Gao, J.-c. (2016). Characterization and photoelectrochemical performance of Zn-doped TiO 2 films by sol–gel method. *Transactions of Nonferrous Metals Society of China, 26*(8), 2109-2116.

Rajput, N. (2015). Methods of preparation of nanoparticles-A review. *International Journal Of Advances In Engineering & Technology, 7*(6), 1806.

Rashidi, A., & Amadeh, A. (2009). The effect of saccharin addition and bath temperature on the grain size of nanocrystalline nickel coatings. *Surface and Coatings Technology, 204*(3), 353-358.

Ren, D., & Haeri, H. (2016). *Advanced Material Science and Engineering (AMSE2016): Proceedings of the 2016 International Conference*: World Scientific.

Roos, J., Celis, J.-P., Fransaer, J., & Buelens, C. (1990). The development of composite plating for advanced materials. *JOM Journal of the Minerals, Metals and Materials Society, 42*(11), 60-63.

Rostami, H., Moghaddam, A. G., & Asgari, R. (2013). Effective lattice Hamiltonian for monolayer MoS 2: Tailoring electronic structure with perpendicular electric and magnetic fields. *Physical Review B, 88*(8), 085440.

Rudnik, E., Burzyńska, L., Dolasiński, Ł., & Misiak, M. (2010). Electrodeposition of nickel/SiC composites in the presence of cetyltrimethylammonium bromide. *Applied Surface Science, 256*(24), 7414-7420.

Rusu, D., Cojocaru, P., Magagnin, L., Gheorghies, C., & Carac, G. (2010). Study of Ni-Tio2 nanocomposite coating prepared by electrochemical deposition. *Journal of optoelectronics and advanced materials, 12*(12), 2419-2422.

Saleh, T. A., & Gupta, V. K. (2012). Synthesis and characterization of alumina nano-particles polyamide membrane with enhanced flux rejection performance. *Separation and Purification Technology, 89*, 245-251.

Schmidt, H. K. (2010). Sol-gel derived nanoparticles as inorganic phases in polymertype matrices.

Schwarz, R., & Johnson, W. (1983). Formation of an amorphous alloy by solid-state reaction of the pure polycrystalline metals. *Physical Review Letters, 51*(5), 415.

Shao, I., Vereecken, P., Cammarata, R., & Searson, P. (2002). Kinetics of particle codeposition of nanocomposites. *Journal of the Electrochemical Society*, *149*(11), C610-C614.

Shao, I., Vereecken, P., Chien, C., Searson, P., & Cammarata, R. (2002). Synthesis and characterization of particle-reinforced Ni/Al 2 O 3 nanocomposites. *Journal of materials research*, *17*(06), 1412-1418.

Shen, T., & Koch, C. (1996). Formation, solid solution hardening and softening of nanocrystalline solid solutions prepared by mechanical attrition. *Acta materialia*, *44*(2), 753-761.

Shen, T., Koch, C., McCormick, T., Nemanich, R., Huang, J., & Huang, J. (1995). The structure and property characteristics of amorphous/nanocrystalline silicon produced by ball milling. *Journal of materials research*, *10*(01), 139-148.

Sherman, A. (1987). Chemical vapor deposition for microelectronics: principles, technology, and applications.

Singh, D. K., & Singh, V. (2012). Electrodeposition and characterization of Ni–TiC composite using N-methylformamide bath. *Materials Science and Engineering: A*, *532*, 493-499.

Singh, V., & Singh, D. (2014). An overview on the preparation, characterization and properties of electrodeposited-metal matrix nanocomposites. *Nanosci. Technol*, *1*(3), 1-20.

Sivaranjani, V., & Philominathan, P. (2016). Synthesize of Titanium dioxide nanoparticles using Moringa oleifera leaves and evaluation of wound healing activity. *Wound Medicine*, *12*, 1-5.

Sk, M. M., Yue, C. Y., Ghosh, K., & Jena, R. K. (2016). Review on advances in porous nanostructured nickel oxides and their composite electrodes for high-performance supercapacitors. *Journal of Power Sources, 308*, 121-140.

Srivastava, M., Grips, V. W., & Rajam, K. (2007). Electrochemical deposition and tribological behaviour of Ni and Ni–Co metal matrix composites with SiC nano-particles. *Applied Surface Science, 253*(8), 3814-3824.

Srivastava, M., Grips, V. W., & Rajam, K. (2008). Influence of SiC, Si 3 N 4 and Al 2 O 3 particles on the structure and properties of electrodeposited Ni. *Materials letters, 62*(20), 3487-3489.

Subramanian, V., Wolf, E. E., & Kamat, P. V. (2003). Influence of metal/metal ion concentration on the photocatalytic activity of TiO2− Au composite nanoparticles. *Langmuir, 19*(2), 469-474.

Surender, M., Basu, B., & Balasubramaniam, R. (2004). Wear characterization of electrodeposited Ni–WC composite coatings. *Tribology International, 37*(9), 743-749.

Suryawanshi, H., Bachhav, S., & Patil, D. (2015). Hydrothermal Synthesis of Zinc Oxide and Its Photocatalytic Effect. *Int. J. Chem. Phys. Sci., 4*, 483-486.

Szczygieł, B., & Kołodziej, M. (2005). Composite Ni/Al 2 O 3 coatings and their corrosion resistance. *Electrochimica Acta, 50*(20), 4188-4195.

Tatsuma, T., Saitoh, S., Ohko, Y., & Fujishima, A. (2001). TiO2− WO3 photoelectrochemical anticorrosion system with an energy storage ability. *Chemistry of materials, 13*(9), 2838-2842.

Teichner, S., Nicolaon, G., Vicarini, M., & Gardes, G. (1976). Inorganic oxide aerogels. *Advances in Colloid and Interface Science, 5*(3), 245-273.

Teymourian, H., Salimi, A., Firoozi, S., Korani, A., & Soltanian, S. (2014). One-pot hydrothermal synthesis of zirconium dioxide nanoparticles decorated reduced graphene oxide composite as high performance electrochemical sensing and biosensing platform. *Electrochimica Acta, 143*, 196-206.

Tiwari, N., Kuraria, R., & Kuraria, S. (2015). Effect of variable trivalent europium concentration on photo-and thermoluminescence of zirconium dioxide nanophosphors. *Materials Science In Semiconductor Processing, 31*, 214-222.

Tjong, S., & Chen, H. (2004). Nanocrystalline materials and coatings. *Materials Science and Engineering: R: Reports, 45*(1), 1-88.

Tjong, S. C. (2007). Novel nanoparticle-reinforced metal matrix composites with enhanced mechanical properties. *Advanced engineering materials, 9*(8), 639-652.

Turner, D. R. (1953). The effect of temperature on the cathode potential during nickel plating. *Journal of The Electrochemical Society, 100*(1), 15-21.

Utamapanya, S., Klabunde, K. J., & Schlup, J. R. (1991). Nanoscale metal oxide particles/clusters as chemical reagents. Synthesis and properties of ultrahigh surface area magnesium hydroxide and magnesium oxide. *Chemistry of Materials, 3*(1), 175-181.

Vacassy, R., Flatt, R., Hofmann, H., Choi, K., & Singh, R. (2000). Synthesis of microporous silica spheres. *Journal of colloid and interface science, 227*(2), 302-315.

Vaezi, M., Sadrnezhaad, S., & Nikzad, L. (2008). Electrodeposition of Ni–SiC nano-composite coatings and evaluation of wear and corrosion resistance and electroplating characteristics. *Colloids and Surfaces A: Physicochemical and Engineering Aspects, 315*(1), 176-182.

Wang, C., Zhong, Y., Ren, W., Lei, Z., Ren, Z., Jia, J., & Jiang, A. (2008). Effects of parallel magnetic field on electrocodeposition behavior of Ni/nanoparticle composite electroplating. *Applied Surface Science*, *254*(18), 5649-5654.

Wang, L. (2008). Effect of surfactant BAS on MoS2 codeposition behaviour. *Journal of Applied Electrochemistry*, *38*(2), 245-249.

Wang, N., Wang, Z., Aust, K., & Erb, U. (1995). Effect of grain size on mechanical properties of nanocrystalline materials. *Acta Metallurgica et Materialia*, *43*(2), 519-528.

Wang, W., Hou, F.-Y., Wang, H., & Guo, H.-T. (2005). Fabrication and characterization of Ni–ZrO 2 composite nano-coatings by pulse electrodeposition. *Scripta Materialia*, *53*(5), 613-618.

Wang, X., Xu, X., & S. Choi, S. U. (1999). Thermal conductivity of nanoparticle-fluid mixture. *Journal of thermophysics and heat transfer*, *13*(4), 474-480.

Weir, A., Westerhoff, P., Fabricius, L., Hristovski, K., & Von Goetz, N. (2012). Titanium dioxide nanoparticles in food and personal care products. *Environmental science & technology*, *46*(4), 2242-2250.

Yadav, T. P., Yadav, R. M., & Singh, D. P. (2012). Mechanical milling: a top down approach for the synthesis of nanomaterials and nanocomposites. *Nanoscience and Nanotechnology*, *2*(3), 22-48.

Yamamoto, H., Otani, Y., Seto, T., Nartpochananon, P., & Charinpanitkul, T. (2012). Generation of uniform tetrapod-shaped zincoxide nanoparticles by gas-phase reaction with using flow restrictor. *Advanced Powder Technology*, *23*(1), 71-79.

Yang, Y., Wen, J., Wei, J., Xiong, R., Shi, J., & Pan, C. (2013). Polypyrrole-decorated Ag-TiO2 nanofibers exhibiting enhanced photocatalytic activity under visible-light illumination. *ACS applied materials & interfaces, 5*(13), 6201-6207.

Yecheskel, Y., Dror, I., & Berkowitz, B. (2013). Catalytic degradation of brominated flame retardants by copper oxide nanoparticles. *Chemosphere, 93*(1), 172-177.

Yoldas, B. E. (1986). Zirconium oxides formed by hydrolytic condensation of alkoxides and parameters that affect their morphology. *Journal of materials science, 21*(3), 1080-1086.

Zhang, D. (2012). Enhancement of the photocatalytic activity of modified TiO 2 nanoparticles with Zn 2+. correlation between structure and properties. *Russian Journal of Physical Chemistry A, Focus on Chemistry, 86*(3), 489-494.

Zhang, S., Sun, D., & Bui, X. L. (2007). Magnetron sputtered hard and yet tough nanocomposite coatings with case studies: nanocrystalline TiN embedded in amorphous SiN X *Nanocomposite Thin Films and Coatings: Processing, Properties and Performance* (pp. 1-110): World Scientific.

Zhang, Y., Wang, L., Liu, B., Zhai, J., Fan, H., Wang, D., Xie, T. (2011). Synthesis of Zn-doped TiO 2 microspheres with enhanced photovoltaic performance and application for dye-sensitized solar cells. *Electrochimica Acta, 56*(18), 6517-6523.